

# GENERATIVE ASSIGNMENT FLOWS FOR REPRESENTING AND LEARNING JOINT DISTRIBUTIONS OF DISCRETE DATA

BASTIAN BOLL, DANIEL GONZALEZ-ALVARADO, STEFANIA PETRA, CHRISTOPH SCHNÖRR

**ABSTRACT.** We introduce a novel generative model for the representation of joint probability distributions of a possibly large number of discrete random variables. The approach uses measure transport by randomized assignment flows on the statistical submanifold of factorizing distributions, which also enables to sample efficiently from the target distribution and to assess the likelihood of unseen data points. The embedding of the flow via the Segre map in the meta-simplex of all discrete joint distributions ensures that any target distribution can be represented in principle, whose complexity in practice only depends on the parametrization of the affinity function of the dynamical assignment flow system. Our model can be trained in a simulation-free manner without integration by conditional Riemannian flow matching, using the training data encoded as geodesics in closed-form with respect to the e-connection of information geometry. By projecting high-dimensional flow matching in the meta-simplex of joint distributions to the submanifold of factorizing distributions, our approach has strong motivation from first principles of modeling coupled discrete variables. Numerical experiments devoted to distributions of structured image labelings demonstrate the applicability to large-scale problems, which may include discrete distributions in other application areas. Performance measures show that our approach scales better with the increasing number of classes than recent related work.

## CONTENTS

1. Introduction	2
1.1. Overview, Motivation	2
1.2. Related Work, Contribution	3
1.2.1. Mathematics, Statistics	3
1.2.2. Own Prior Work	3
1.2.3. Machine Learning	4
1.2.4. Closely Related Work	5
1.2.5. Contribution: Summary	5
1.3. Organization	6
2. Background	6
2.1. Assignment Flows	6
2.2. Meta-Simplex Flow Embedding	8
3. Approach	9
3.1. Generative Model	9
3.2. Representation of Labelings as Training Data	11
3.3. Riemannian Flow Matching	11
3.3.1. Training Criterion	11

2010 *Mathematics Subject Classification.* 49Q22, 53B12, 62H35, 68T05, 68U10, 91A22.

*Key words and phrases.* generative models, discrete random variables, normalizing flows, information geometry, neural ODEs, assignment flows, replicator equation.

This work was funded by the Deutsche Forschungsgemeinschaft (DFG), grant SCHN 457/17-1, within the priority programme SPP 2298: Theoretical Foundations of Deep Learning. This work was funded by the Deutsche Forschungsgemeinschaft (DFG) under Germany's Excellence Strategy EXC-2181/1-390900948 (the Heidelberg STRUCTURES Excellence Cluster).

3.3.2. Construction of Conditional Fields	12
3.3.3. Infinite Integration Time	15
3.3.4. Relation to Dirichlet Flow Matching	15
3.4. Learning Interaction between Simplices	16
3.5. Numerical Flow Integration	19
3.6. Likelihood Computation	19
3.7. Dequantization	20
4. Experiments and Discussion	21
4.1. Class Scaling	21
4.2. Generating Image Segmentations	21
4.3. Likelihood Evaluation	22
5. Conclusion	23
Appendix A. Experiments: Details	24
A.1. Details of Class Scaling Experiment	24
A.2. Details of generating Image Segmentation	24
A.2.1. Cityscapes Data Preparation	24
A.2.2. Cityscapes Training	24
A.2.3. Binarized MNIST Data Preparation	25
A.2.4. Binarized MNIST Training	25
Appendix B. Likelihood Computation: Details	25
References	29

## 1. INTRODUCTION

**1.1. Overview, Motivation.** *Generative models* in machine learning define an active area of research [KPB21, PNR<sup>+</sup>21, RH21]. Corresponding research objectives include

- (i) the representation of complex probability distributions,
- (ii) efficient sampling from such distributions, and
- (iii) computing the likelihoods of unseen data points.

The target probability distribution is typically not given, except for a finite sample set (empirical measure). The modeling task concerns the generation of the target distribution by transporting a simple reference measure, typically the multivariate standard normal distribution, using a smooth diffeomorphism. The latter is realized by a network with trainable parameters that are optimized by maximizing the likelihood of the given data or a corresponding surrogate objective which is more convenient regarding numerical optimization. This class of approaches are called *normalizing flows* in the literature.

This paper is concerned with the significant subclass of *discrete (categorical)* probability distributions of  $n$  random variables taking values in the finite set  $[c]$ ,

$$y = (y_1, \dots, y_n)^\top \in [c]^n, \quad y_i \in [c] := \{1, 2, \dots, c\}, \quad i \in [n], \quad c, n \in \mathbb{N}. \quad (1.1)$$

A corresponding distribution  $p$  is a look-up table which specifies for any realization  $\alpha$  of the discrete random vector  $y$  the probability

$$p(\alpha) = p(\alpha_1, \dots, \alpha_n) := \Pr(y = \alpha) = \Pr(y_1 = \alpha_1 \wedge \dots \wedge y_n = \alpha_n), \quad \alpha \in [c]^n. \quad (1.2)$$

Thus any discrete distribution  $p$  is a nonnegative tensor with the combinatorially large number of

$$N := c^n \quad (1.3)$$

entries. Furthermore, since  $\sum_{\alpha \in [c]^n} p(\alpha) = 1$ , any distribution  $p$  corresponds to a point of the probability simplex

$$\Delta_N = \{p \in \mathbb{R}_{\geq 0}^N : \langle \mathbb{1}_N, p \rangle = 1\}, \quad p = (p_\alpha)_{\alpha \in [c]^n}, \quad p_\alpha = p(\alpha). \quad (1.4)$$

Such distributions abound in applications (Section 1.2), yet have received less attention in the literature on generative models. The recent survey paper [KPB21] concludes with a short paragraph devoted to discrete distributions and the assessment that “the generalization of normalizing flows to discrete distributions remains an open problem”. Likewise, the survey paper [PNR<sup>+</sup>21] discusses briefly generative models of discrete distributions in Section 5.3. Authors state that “compared to flows on  $\mathbb{R}^D$ , discrete flows have notable theoretical limitations”. The survey paper [RH21] does not mention at all generative models of discrete distributions.

This paper introduces a novel generative model tailored to discrete distributions

- by pushing forward a simple reference distribution on a submanifold of discrete measures which ‘spans’ the entire simplex (1.4);
- by determining the parameters of the generative map through matching the flow of a corresponding dynamical system to closed-form geodesics encoding training data.

Figure 1.1 illustrates the approach for the toy distribution of two binary variables

$$p(\alpha_1, \alpha_2): \begin{array}{c|cc} \alpha_1/\alpha_2 & 0 & 1 \\ \hline 0 & 0.45 & 0.05 \\ \hline 1 & 0.05 & 0.45 \end{array} \quad (1.5)$$

The simplex  $\Delta_4 \subset \mathbb{R}^4$  (1.4) is visualized in  $\mathbb{R}^3$  in local coordinates as tetrahedron. The generative model only uses the submanifold of *factorizing* discrete distributions which ensures computational efficiency of both training and sampling. Sampling is done by computing the integral curve of random initial points, each of which converges to a vertex corresponding to a realization  $\alpha$ .

## 1.2. Related Work, Contribution.

1.2.1. *Mathematics, Statistics.* Joint distributions of discrete random variables have a long history in multivariate statistics [Agr13]. This includes the study of subsets of such distributions known as *discrete graphical models* [Lau96, CDLS99, KF09]. Here, conditional independency assumptions encoded by the structure of an underlying graph [Stu05] effectively reduce the degree of freedoms (1.3) of general discrete distributions and imply factorization of  $p$  once realizations of conditioning variables are observed. From the algebraic viewpoint, such statistical assumptions about  $p$  give rise to monomial constraints. The study of the topology and geometry of the resulting algebraic varieties which support corresponding subfamilies of distributions, is the subject of the fields of *algebraic statistics* [GMS06, LSX09, DSS09, Zwi16, Sul18]. In fact, the special case of fully factorizing discrete distributions

$$p(\alpha) = \prod_{i \in [n]} p_i(\alpha_i) \quad (1.6)$$

is particularly relevant for this paper. For example, the subfamily of all such distributions, in the case  $n = c = 2$ , is depicted by Figure 1.1 and known as as Wright manifold in mathematical game theory [HS98] and more generally as *Segre variety*  $\Sigma_{1,1}$  in algebraic geometry [Har92, Lan12].

1.2.2. *Own Prior Work.* Our approach utilizes *assignment flows* [ÅPSS17] whose flow evolves on the product of the relative interiors of the probability simplices  $\Delta_c$ , called *assignment manifold*, one factor for each random variable  $y_i$ ,  $i \in [n]$ . The restriction to strictly positive discrete distribution with full support enables to turn these domains into elementary statistical manifolds equipped with the Fisher-Rao geometry and the

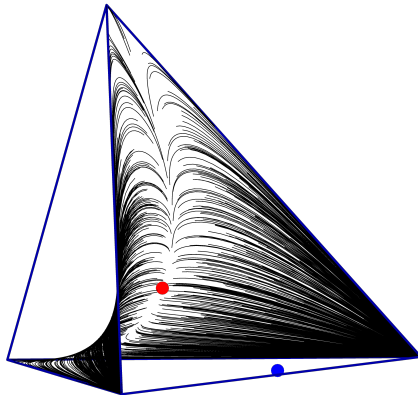


FIGURE 1.1. Visualization of 1000 samples from the target distribution  $p(\alpha_1, \alpha_2)$  given by (1.5), corresponding to the blue point in the meta-simplex  $\mathcal{S}_N$ ,  $N = c^n = 4$ , with  $n = 2$  binary random variables  $y_1, y_2$ , each taking  $c = 2$  values. Each sample corresponds to an integral curve  $T(W(t))$  (2.20) of the assignment flow ODE (2.10) on the embedded submanifold of factorizing distributions  $\mathcal{W} \subseteq \mathcal{S}_4$ , which can be computed efficiently by geometric integration. The entire assignment flow pushes forward a standard Gaussian reference distribution on the tangent space  $T_0$  (not shown) at the barycenter (red point), which is lifted to the submanifold and transported to the extreme points. The resulting ‘weights’ represent the blue target distribution as convex combination. The parametrized vector field of the generative model is trained in a stable and efficient way by matching e-geodesic curves on the assignment manifold, which represent the training data and can be computed in closed form.

e-connection of information geometry [AN00]. The corresponding exponential map and the geodesics can be specified in closed form.

This paper introduces the following approach to devising a generative model for discrete random variables: Geometric integration of the assignment flow realizes a map which pushes forward a standard reference measure on the tangent space at the barycenter to an extreme point of the (closure) of the assignment manifold. By embedding the assignment manifold into the simplex (1.4) of all discrete joint distributions using the Segre map, the pushforward measure concentrates on the extreme points and hence represents a more complex *non-factorizing* discrete joint distribution by convex combination of Dirac measures, each of which corresponds to a realization  $\alpha \in [c]^n$ . Figure 3.1 provides a schematic overview.

Our recent work [BCA<sup>+</sup>24] characterizes assignment flows as multi-population games and studies multi-game dynamics via the aforementioned embedding approach. Results established in this work will be employed in Section 3.4.

1.2.3. *Machine Learning.* The aforementioned negative statements in the survey papers [KPB21, PNR<sup>+</sup>21] about generative models for discrete distributions have stimulated corresponding research recently, in the field of machine learning. We refer to [BGAS24, Section 2.2] for a discussion which we do not repeat here. To the best of our knowledge, none of these approaches is directly tailored to discrete distributions like our approach based on a corresponding Riemannian statistical manifold (see Section 1.2.4 for a discussion of papers which appeared during writing this manuscript). Likewise, the very fact that distributions (1.2) are nonnegative tensors suggest connections to the corresponding literature and low-rank approximations [KB09, GKT13, Hac14]. For example, factorizing multivariate functions have been used for multivariate function approximation (e.g., [BGM09]), and tensorization of rank-1 tensors in order to represent higher-rank

tensors [KB09] are similar to Segre embeddings from algebraic geometry. Yet, both the context (generative models) and our geometric approach distinguish our approach.

Regarding the training of our generative model, our approach builds on the recent work [LCBH<sup>+</sup>23, CL23]. The authors introduced a *flow-matching approach* to the training of continuous generative models which enables more stable and efficient training and hence an attractive alternative to established maximum likelihood training. In this paper, we adopt this criterion and adapt it to our generative model for discrete distributions. In particular, we encode given training data as e-geodesics on the assignment manifold which makes flow matching convenient and effective.

1.2.4. *Closely Related Work.* During the preparation of this manuscript, two papers appeared which also adopt flow matching for learning generative models for discrete distributions. The paper [SJW<sup>+</sup>24] employs the parametric Dirichlet distribution on the probability simplex [Fer73, JK77, Ait82] as intermediate conditional distributions in a flow matching approach. A similarity to our method is the use of infinite transport time, which achieves favorable scaling in the regime of many classes. We get back to this paper for a more detailed comparison in Section 3.3.4.

The second paper [DKP<sup>+</sup>24] essentially takes up our approach [BGAS24] except for using geodesics with respect to the Riemannian connection rather than the e-connection, corresponding to  $\alpha = 0$  and  $\alpha = 1$  in the family of  $\alpha$ -connections, respectively. As explained in [ÅPSS17, Lemma 1] by virtue of the sphere map [ÅPSS17, Def. 1] as isometry, the former geodesics correspond to the geodesics (great circles) on the sphere with radius 2, restricted to the intersection with the open positive orthant. The authors of [DKP<sup>+</sup>24] argue that their choice avoids numerical instability at the boundary of the manifold, which is true when working on the sphere. But this issue does not exist either on the simplex when proper geometric numerical integration schemes are employed [ZSPS20].

Possible drawbacks when working on the sphere are not addressed in [DKP<sup>+</sup>24]. The boundary of the manifold is reached along geodesics paths in *finite* time and samples generated by a *learned* generative model may potentially *leave* the manifold. This cannot occur when working with e-geodesics which constitute a first-order approximation of the Riemannian geodesics [ÅPSS17, Prop. 3], and with the corresponding exponential map whose domain is the *entire* tangent space. In this sense, the simplex equipped with both the Fisher-Rao metric and the e-connection behaves effectively like a complete manifold, even though it is not complete (e.g. closed) mathematically. This is quite convenient for both numerical inference and learning.

The authors of [DKP<sup>+</sup>24] also claim ‘to leverage Riemannian optimal transport’ for improving the training dynamics. From the mathematical viewpoint, the presentation of this aspect is not made sufficiently explicit and the pertinent literature is ignored. Besides standard textbooks about optimal transport [Vil09, San15], we refer to [LM18] for a thorough study of the geometry on the simplex induced by the Wasserstein distance. In fact, the ‘natural gradient’ descent form presented as Equation (8) in [DKP<sup>+</sup>24, Prop. 1] is closely related to Equation (15) in [LM18], and the difference to the Fisher-Rao geometry is pointed out as Remark 2 in [LM18].

Finally, we refer to another line of research concerned with the approximation of discrete probability distributions by continuous distributions, called *dequantization* [UML13, TvDOB16, DSDB17, SKCK17, HCS<sup>+</sup>19]. A dequantization approach for general discrete data, i.e. similar in scope to our approach, was recently proposed by [CAN22]. We get back to this paper in Section 3.7 and provide a detailed comparison by characterizing our approach as dequantization procedure and pointing out differences. In particular, we indicate that a key component of the approach [CAN22], learning an embedding of class configurations, can be replicated using our approach, by defining an extended payoff function of the generative assignment flow approach.

1.2.5. *Contribution: Summary.* Summing up, the generative model introduced in this paper seamlessly combines a flow-matching approach with a Riemannian geometric structure tailored to represent discrete

distributions and to generate discrete and categorical data. A preliminary announcement of our approach is [BGAS24]. The present paper considerably elaborates this work regarding the presentation of the approach, mathematical details, experiments and discussion of closely related work.

**1.3. Organization.** Section 2 fixes notation, summarizes the assignment flow approach and the embedding into the meta-simplex (1.4). The core Section 3 introduces and details our approach. The flow-matching approach is described in Section 3.3 and how it relates to the recent work [LCBH<sup>+</sup>23, CL23] which inspired the training component of our approach. Section 3.5 details the particular geometric integration used in all experiments, for computing the assignment flow within the framework worked out by [ZSPS20]. Section 3.6 explains how the trained generative model is evaluated for computing the likelihoods of a novel unseen data points. A range of experimental results are presented and discussed in Section 4. We conclude in Section 5.

## 2. BACKGROUND

**2.1. Assignment Flows.** Let  $(X, d)$  denote a metric space and  $\mathcal{X}_m = \{(x_1, y_1), \dots, (x_m, y_m)\}$  given *labeled* data: each sample indexed by  $k \in [m]$ ,

$$x_k \in X^n, \quad x_k = \{x_{k1}, \dots, x_{kn}\}, \quad x_{ki} \in X, \quad i \in \mathcal{V}(\mathcal{G}) = [n], \quad k \in [m] \quad (2.1)$$

comprises data points  $x_{ki}$  observed at vertices  $i \in \mathcal{V} = \mathcal{V}(\mathcal{G})$  of an underlying graph  $\mathcal{G} = (\mathcal{V}, \mathcal{E})$ , that carry the label  $y_i \in [c]$  for some given number  $c \in \mathbb{N}$  of class labels. Assignment flows [ÅPPS17, Sch20] denote a class of dynamical systems for the assignment of labels to data points  $x = (x_1, \dots, x_n)$ ,

$$[c] \ni y_i \mapsto x_i \in X, \quad i \in [n], \quad (2.2)$$

called *labeling* of  $x$ . Denote by

$$\mathcal{S}_c := \mathring{\Delta}_c = \{p \in \mathbb{R}^c : p_j > 0, \langle \mathbb{1}_c, p \rangle = 1, \forall j \in [c]\} \quad (2.3)$$

the relative interior of the probability simplex which, equipped with the **Fisher-Rao metric**

$$g_p(u, v) := \langle u, \text{Diag}(p)^{-1}v \rangle, \quad u, v \in T_0, \quad p \in \mathcal{S}_c \quad (2.4a)$$

$$T_0 := T_0\mathcal{S}_c := \{v \in \mathbb{R}^c : \langle \mathbb{1}_c, v \rangle = 0\} \quad (2.4b)$$

becomes the Riemannian manifold  $(\mathcal{S}_c, g)$  with trivial tangent bundle  $T\mathcal{S}_c = \mathcal{S}_c \times T_0$ . Corresponding to the vertices  $\mathcal{V}$  of the underlying graph  $\mathcal{G}$ , we define the product manifold

$$\mathcal{W} := \mathcal{S}_c \times \dots \times \mathcal{S}_c, \quad (n = |\mathcal{V}| \text{ factors}) \quad (2.5a)$$

$$\mathcal{T}_0 := T_0\mathcal{W} := T_0 \times \dots \times T_0, \quad (n = |\mathcal{V}| \text{ factors}) \quad (2.5b)$$

with points denoted by

$$\mathcal{W} \ni W = (W_1, \dots, W_n)^\top \in \mathbb{R}_{>}^{n \times c}, \quad W_i \in \mathcal{S}_c, \quad i \in [n] \quad (2.6a)$$

$$\mathcal{T}_0 \ni V = (V_1, \dots, V_n)^\top \in \mathbb{R}^{n \times c}, \quad V_i \in T_0, \quad i \in [n]. \quad (2.6b)$$

Specifically, we denote by

$$\mathbb{1}_{\mathcal{W}} = (\mathbb{1}_{\mathcal{S}}, \dots, \mathbb{1}_{\mathcal{S}})^\top, \quad \mathbb{1}_{\mathcal{S}} := \frac{1}{c} \mathbb{1}_c \in \mathcal{S}_c \quad (2.7)$$

the **barycenter** of  $\mathcal{W}$ , where  $\mathbb{1}_{\mathcal{S}}$  is the barycenter of  $\mathcal{S}_c$  defined by (2.3). The orthogonal projections onto  $T_0$  and  $\mathcal{T}_0$ , respectively, are denoted by

$$\pi_0 : \mathbb{R}^c \rightarrow T_0, \quad \pi_0 := I_c - \mathbb{1}_c \mathbb{1}_{\mathcal{S}}^\top, \quad (2.8a)$$

$$\Pi_0 : \mathbb{R}^{n \times c} \rightarrow \mathcal{T}_0, \quad \Pi_0 U := (\pi_0 U_1, \dots, \pi_0 U_n)^\top. \quad (2.8b)$$

$\mathcal{W}$  equipped with the **Fisher-Rao product metric**

$$g_W(U, V) = \sum_{i \in [n]} g_{W_i}(U_i, V_i), \quad (2.9)$$

where the right-hand side is defined by (2.4a), becomes the Riemannian manifold  $(\mathcal{W}, g)$  called **assignment manifold**, with trivial tangent bundle  $T\mathcal{W} = \mathcal{W} \times \mathcal{T}_0$ . *Assignment flows* are dynamical systems of the general form

$$\dot{W}(t) = R_{W(t)}[F_\theta(W(t))], \quad W(0) = W_0 \in \mathcal{W}, \quad (\text{assignment flow}) \quad (2.10)$$

where

$$F_\theta: \mathcal{W} \rightarrow \mathbb{R}^{n \times c} \quad (2.11)$$

denotes an arbitrary function with parameters  $\theta$ . The linear mapping  $R_W$  acts row-wise by

$$R_W[F_\theta] := (\dots, R_{W_i}F_{\theta,i}, \dots)^\top \quad (2.12a)$$

$$R_{W_i}F_{\theta,i} = (\text{Diag}(W_i) - W_iW_i^\top)F_{\theta,i}, \quad W_i \in \mathcal{S}_c, \quad F_{\theta,i} \in \mathbb{R}^c, \quad i \in [n]. \quad (2.12b)$$

Since the range  $\mathcal{R}(R_{W_i}) = T_0$  for any  $W_i \in \mathcal{S}_c$ , the assignment flow (2.10) is well-defined. The data point  $x = (x_1, \dots, x_n) \in X^n$  to be labeled, is encoded by the initial point  $W_0$  in (2.10). The label assignment (2.2) is accomplished by solving the assignment flow equation (2.10), since

$$\lim_{t \rightarrow \infty} W_i(t) = e_{y_i}, \quad y_i \in [c], \quad \forall i \in [n], \quad (2.13)$$

where  $e_{y_i} = (0, \dots, 0, 1, 0, \dots, 0)^\top \in \{0, 1\}^c$  denotes the unit vector with a single entry 1 at the position  $y_i$ , corresponding to the assignment of the label  $y_i$  to the component  $x_i$  of  $x$  at vertex  $i \in [n]$ .

Assignment flows have been introduced in [ÅPSS17] with basic properties (well-posedness, convergence) established in [ZZS22] under suitable assumptions. A wide range of efficient geometric integration schemes exist for computing  $W(t)$  [ZSPS20] (see also Section 3.5 below).

We conclude this section by collecting formulas required for the specification of e-geodesic flows in subsequent sections. We refer to [AN00] for more details on information geometry. The *exponential map* with respect to the e-connection reads

$$\text{Exp}_p(v) = \frac{p \cdot e^{\frac{v}{p}}}{\langle p, e^{\frac{v}{p}} \rangle}, \quad p \in \mathcal{S}_c, \quad v \in T_0, \quad (2.14)$$

where both the multiplication  $\cdot$  and the exponential function apply componentwise. We define the *lifting map* [ÅPSS17]

$$\exp_p: T_0 \rightarrow \mathcal{S}_c, \quad p \in \mathcal{S}_c, \quad (2.15a)$$

$$\exp_p := \text{Exp}_p \circ R_p. \quad (\text{lifting map}) \quad (2.15b)$$

Both mappings (2.14) and (2.15) extend factor-wise to the product space  $\mathcal{T}_0$  given by (2.5b), analogous to (2.12). We denote by

$$\mathcal{P}(\mathcal{W}) \quad (2.16)$$

the set of probability measures supported on the assignment manifold  $\mathcal{W}$ .

**2.2. Meta-Simplex Flow Embedding.** The set of categorical distribution represented by the assignment manifold  $\mathcal{W}$  (2.5a) only forms the small subset of *fully factorized* distributions among the set of *all* categorical distributions of  $c$  labels on  $n$  vertices, given by the *meta-simplex*<sup>1</sup>

$$\mathcal{S}_N := \overset{\circ}{\Delta}_N = \{p \in \mathbb{R}^N : p_j > 0, \langle \mathbb{1}_N, p \rangle = 1, \forall j \in [N]\} \quad \text{with} \quad N = c^n. \quad (2.17)$$

Every extreme point of the closure  $\Delta_N = \overline{\mathcal{S}_N}$  is a unit vector  $e_j$ ,  $j \in [N]$  which encodes a single labeling on the *entire* graph. Rather than using  $j \in [N]$ , it will be convenient to enumerate and index the combinatorially large number  $N = c^n$  of all labelings by the multi-indices

$$\alpha \in [c]^n, \quad \alpha = (\alpha_1, \dots, \alpha_n), \quad \alpha_i \in [c], \quad i \in [n]. \quad (2.18)$$

Thus, any  $\alpha$  is a *label configuration* which indexes an extreme point  $e_\alpha \in \Delta_N$  of the meta-simplex (unit vector, discrete Dirac measure) and corresponds to a hard category or *label assignment* (2.2) in terms of a realization of each discrete random variable  $y_1, \dots, y_n$ . The components of a point  $p \in \mathcal{S}_N$  in (2.17) are indexed by  $\alpha$  as well, and we will use the notations

$$p_\alpha := p(\alpha) = p(\alpha_1, \dots, \alpha_n) = \Pr(y = \alpha), \quad \alpha \in [c]^n. \quad (2.19)$$

A key component of our approach will be the embedding of the assignment manifold  $\mathcal{W} \hookrightarrow \mathcal{S}_N$  of the assignment manifold (2.5a) into the meta-simplex (2.17). The embedding map

$$T: \mathcal{W} \rightarrow \mathcal{T} = T(\mathcal{W}) \subset \mathcal{S}_N, \quad T(W)_\alpha := \prod_{i \in [n]} W_{i, \alpha_i}, \quad \alpha \in [c]^n \quad (2.20)$$

as well as the map

$$Q: \mathbb{R}^{n \times c} \rightarrow \mathbb{R}^N, \quad Q: T_0\mathcal{W} \rightarrow T_0\mathcal{S}_N, \quad (QV)_\alpha := \sum_{i \in [n]} V_{i, \alpha_i}, \quad \alpha \in [c]^n \quad (2.21)$$

which will later on play the role corresponding to  $T$  for tangent vectors, have been introduced and studied in [BSGA<sup>+</sup>23, BCA<sup>+</sup>24]. Every point  $W \in \mathcal{W}$  on the assignment manifold is represented by the combinatorially large vector  $T(W)$  with  $N = c^n$  components  $T(W)_\alpha$ , consisting of monomials of degree  $n$  in the variables  $W_{i, \alpha_i} \in (0, 1)$ . A labeling determined by the assignment flow by (2.13) corresponds to  $\lim_{t \rightarrow \infty} T(W(t)) = T(\overline{W}) = e_\alpha$  with exactly one single non-zero component  $T(\overline{W})_\alpha = 1$ .

**Example 2.1.** Consider the case  $n = c = 2$ . Then  $N = 4$  and the meta-simplex  $\mathcal{S}_N$  contains all joint distributions  $p(y_1, y_2)$  of two binary random variables. If  $p(y_1, y_2) = W$  is a point on the assignment manifold, however, then  $W = \left( \begin{pmatrix} w_1 \\ 1-w_1 \end{pmatrix}, \begin{pmatrix} w_2 \\ 1-w_2 \end{pmatrix} \right)^\top$ . Embedding this point by (2.20) yields the vector  $T(W) = (w_1 w_2, w_1(1-w_2), (1-w_1)w_2, (1-w_1)(1-w_2))^\top$ , with components  $T(W)_\alpha$  indexed by  $\alpha \in \{(1, 1), (1, 0), (0, 1), (0, 0)\}$ . Since any distribution on the assignment manifold factorizes, this vector is determined by merely two parameters. Accordingly, the embedded assignment manifold  $\mathcal{T} = T(\mathcal{W}) \subset \mathcal{S}_N$  is the two-dimensional submanifold depicted by Figure 2.1. From the viewpoint of mathematics, such embedded sets are known as *Segre varieties* at the intersection of algebraic geometry and statistics [LSX09, DSS09].

The following proposition highlights the specific role of the embedded assignment manifold  $\mathcal{T} = T(\mathcal{W}) \subset \mathcal{S}_N$ .

**Proposition 2.2** ([BCA<sup>+</sup>24, Prop. 3.2]). *For every  $W \in \mathcal{W}$ , the distribution  $T(W) \in \mathcal{S}_N$  has maximum entropy*

$$H(T(W)) = - \sum_{\alpha \in [c]^n} T(W)_\alpha \log T(W)_\alpha \quad (2.22)$$

<sup>1</sup>We call ‘meta-simplex’ both  $\Delta_N = \overline{\mathcal{S}_N}$  and the subset  $\mathcal{S}_N \subset \Delta_N$  of distributions with full support.

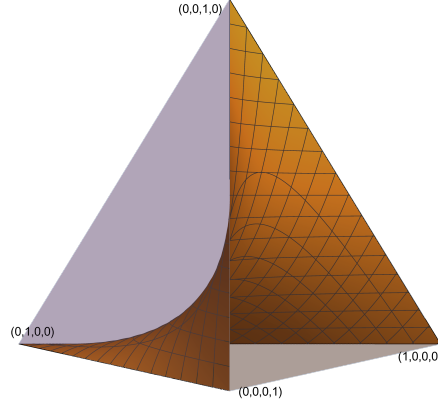


FIGURE 2.1. Visualization of  $\mathcal{T} = T(\mathcal{W}) \subset \mathcal{S}_N$  for  $n = c = 2$  (Example 2.1).

among all  $p \in \mathcal{S}_N$  subject to the marginal constraint

$$Mp = W, \quad (2.23a)$$

where the marginalization map  $M: \mathbb{R}^N \rightarrow \mathbb{R}^{n \times c}$  is given by

$$(Mp)_{i,j} := \sum_{\alpha \in [c]^n: \alpha_i=j} p_\alpha, \quad \forall (i,j) \in [n] \times [c]. \quad (2.23b)$$

Any *general* distribution  $p \in \mathcal{S}_N \setminus T(\mathcal{W})$  which is *not* in  $T(\mathcal{W})$  has *non*-maximal entropy and hence is *more* informative by encoding additional statistical dependencies [CT06]. Our approach for generating general distributions  $p \in \mathcal{S}_N$ , by combining simple distributions  $W \in \mathcal{W}$  via the embedding (2.20) and assignment flows (2.10), is introduced in Section 3.

### 3. APPROACH

This section introduces our generative model for representing and learning a discrete joint distribution  $p \in \mathcal{S}_N$  (recall the notation (2.19)) of label configurations as realizations of discrete random variables  $y_1, \dots, y_n$ . The approach is illustrated by Figure 3.1.

**3.1. Generative Model.** The goal is to learn an approximation  $\tilde{p} \approx p$ , as convex combination of factorizing joint distributions. The submanifold  $\mathcal{T} = T(\mathcal{W}) \subseteq \mathcal{S}_N$  shown in Figure 2.1 spans all factorizing distributions  $T(W) \in \mathcal{S}_N$ , which are efficiently represented by their marginals  $W \in \mathcal{W}$ . In particular, since the dimension of  $\mathcal{W}$  only grows linearly in the number of variables  $n$ , factorizing distributions are tractable to work with numerically. However, only independent random variables follow factorizing distributions, posing the question of how coupling can be represented through convex combination.

First, note that  $\mathcal{T} \subseteq \mathcal{S}_N$  is not a convex set. Thus, the convex combination of two factorizing distributions  $T(W_1)$  and  $T(W_2)$  generally lies outside of  $\mathcal{T}$ . In addition, every Dirac measure  $e_\alpha$  factorizes. Intuitively, this is because each variable has a deterministic value, independent of all others, and it corresponds to the fact that (the closure of)  $\mathcal{T}$  spans all extreme points of  $\mathcal{S}_N$  (see Figure 2.1). Because Dirac measures are the extreme points of the convex set  $\mathcal{S}_N$ , every joint distribution  $\tilde{p} \in \mathcal{S}_N$  representing an *arbitrary* coupling between variables can be written as a convex combination of Dirac measures

$$\tilde{p} = \sum_{\alpha \in [c]^n} \tilde{p}_\alpha e_\alpha. \quad (3.1)$$

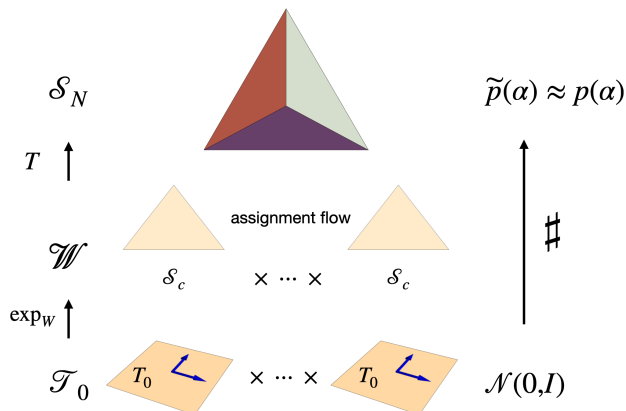


FIGURE 3.1. **Overview of the approach:** The standard Gaussian reference measure  $\mathcal{N}(0, I)$  is pushed forward by the exponential map  $\text{exp}_W$  from the flat tangent product space  $\mathcal{T}_0$  to the assignment manifold  $\mathcal{W}$ , and further to the meta-simplex  $\mathcal{S}_N$  (2.17) by geometrically integrating the assignment flow (2.10). Since the assignment flow converges to the extreme points of  $\overline{\mathcal{W}}$  which agree with the extreme points of  $\Delta_N = \overline{\mathcal{S}_N}$ , an approximation  $\tilde{p}(\alpha)$  of a general *discrete* target measure  $p(\alpha)$  underlying given data can be learned by matching the flow of e-geodesics (corresponding to data samples) and convex combination, in terms of factorized distributions  $T(W)$ ,  $W \in \mathcal{W}$  embedded as submanifold of  $\mathcal{S}_N$  (Figure 2.1) and empirical expectation.

This particular representation of  $\tilde{p}$  is intractable, however, because it involves a combinatorial number of mixture coefficients  $\tilde{p}_\alpha$ . To tame this complexity, we propose to represent mixtures  $\tilde{p} \in \mathcal{S}_N$  of factorizing distributions as measures  $\nu \in \mathcal{P}(\mathcal{W})$  by

$$\tilde{p} = \mathbb{E}_{W \sim \nu}[T(W)]. \quad (3.2)$$

This shifts the problem of parameterizing useful subsets of combinatorially many mixture coefficients in (3.1) to the problem of parameterizing a preferably large subset of measures  $\nu \in \mathcal{P}(\mathcal{W})$ , supported on the comparatively low-dimensional manifold  $\mathcal{W}$ . The latter can be achieved by parameterized measure transport on the assignment manifold. A simple reference measure  $\nu_0 \in \mathcal{P}(\mathcal{W})$  is chosen and transported by the assignment flow (2.10), reaching  $\nu = \nu_\infty$  for  $t \rightarrow \infty$ . Parameterization of measures  $\nu_\theta \in \mathcal{P}(\mathcal{W})$  is thus achieved by choosing an appropriate class of payoff functions  $F_\theta: \mathcal{W} \rightarrow \mathbb{R}^{n \times c}$  driving the assignment flow (2.10).

Note that, while the support of  $\tilde{p}$  in (3.1) was directly associated with the number of mixture coefficients, the complexity of representing  $\tilde{p}$  via the ansatz (3.2) is no longer associated with its support. For example, the simplest instance of (3.2), choosing  $F_\theta \equiv 0$ ,  $\nu = \nu_0$  for a product reference distribution  $\nu_0 = \hat{\nu}_0^n$  with mean  $\mathbb{E}_{W_i \sim \hat{\nu}_0}[W_i] = \mathbb{1}_{\mathcal{S}_c}$ , leads to  $\tilde{p} = \mathbb{1}_{\mathcal{S}_N}$ . This is the uniform distribution over class configurations, which has full support. To see that  $\hat{\nu}_0^n$  indeed represents  $\mathbb{1}_{\mathcal{S}_N}$  via (3.2), we show the following lemma.

**Lemma 3.1 (nodewise measures).** *Let  $\nu = \prod_{i \in [n]} \hat{\nu}_i$  for measures  $\hat{\nu}_i \in \mathcal{P}(\mathcal{S}_c)$ . Then the joint distribution represented by the mixture (3.2) reads*

$$\tilde{p} = \mathbb{E}_{W \sim \nu}[T(W)] = T(\widehat{W}), \quad \widehat{W}_i = \mathbb{E}_{W_i \sim \hat{\nu}_i}[W_i], \quad i \in [n]. \quad (3.3)$$

*Proof.* Let  $\alpha \in [c]^n$  be an arbitrary multi-index. Since  $\nu$  factorizes in the described manner,  $W \sim \nu$  is independently distributed on each node which implies

$$\tilde{p}_\alpha = \mathbb{E}_{W \sim \nu}[T(W)_\alpha] = \mathbb{E}_{W \sim \nu} \left[ \prod_{i \in [n]} W_{i, \alpha_i} \right] = \prod_{i \in [n]} \mathbb{E}_{W \sim \tilde{\nu}_i}[W_{i, \alpha_i}] = T(\widehat{W})_\alpha. \quad (3.4)$$

□

Lemma 3.1 shows that, if  $\nu$  is independent on every node, then  $\tilde{p} \in \mathcal{T}$ . In the following, the reference measure  $\nu_0$  will have this independence property, which illustrates that coupling between variables, represented in the joint distribution  $\tilde{p}$ , is necessarily induced by interaction between node states over the course of integrating the assignment flow.

In practice, the target distribution  $p$  is unknown and only independently drawn training samples  $\beta \sim p$  are available. After choosing a class of payoff functions  $F_\theta$ , the task is to learn parameters  $\theta$  such that  $\tilde{p} = \mathbb{E}_{W \sim \nu_\theta}[T(W)]$  approximates the empirical distribution of samples. To this end, we identify samples  $\beta$  with the corresponding extremal points  $Me_\beta \in \overline{\mathcal{W}}$  (Section 3.2) and use *flow matching* on  $\mathcal{W}$  to learn  $\theta$  in a numerically stable and efficient way (Section 3.3).

After learning has converged, new samples from  $\tilde{p} \approx p$  can be drawn by a two-stage process. First, an initialization  $W_0 \sim \nu_0$  is drawn and evolved over time  $W(t) \in \mathcal{W}$  by following the learned assignment flow until either the desired time  $t_{\max}$  is reached, or  $W(t)$  approaches an extreme point of  $\mathcal{W}$ . The new data is subsequently drawn from the factorizing distribution  $T(W(t_{\max}))$ . At extreme points  $Me_{\beta'}$ , this distribution is a Dirac measure and sampling from it always yields  $\beta'$ . Finally, we specify the geometric integration method that we employed for the discretization of our time-continuous generative model in numerical experiments (Section 3.5), and the computation of the likelihood  $\tilde{p}(\alpha)$  of arbitrary label configurations using the learned generative model (Section 3.6).

**3.2. Representation of Labelings as Training Data.** Our approach to training the generative model, to be introduced in Section 3.3, utilizes *labelings* as training data of the form

$$\overline{W} \in \overline{\mathcal{W}}, \quad \overline{W}_i = e_{\alpha_i}, \quad \alpha_i \in [c], \quad \forall i \in [n]. \quad (3.5)$$

Any such point  $\overline{W}$  assigns a label (category)  $\alpha_i$  to each vertex  $i \in \mathcal{V}$  in terms of a corresponding unit vector  $e_{\alpha_i} \in \{0, 1\}^c$ . The flow-matching criterion, specified in the following section, is optimized to find  $\theta$  such that  $F_\theta$  drives the assignment flow to labelings in the limit  $\lim_{t \rightarrow \infty} W(t) = \overline{W}$ . In practice, the assignment flow is integrated up to a sufficiently large point of time

$$t_{\max} > 0 \quad (3.6)$$

followed by trivial rounding of  $W_i(t_{\max}) \mapsto e_{\alpha_i}$  at every vertex  $i$ .

### 3.3. Riemannian Flow Matching.

**3.3.1. Training Criterion.** This section details the approach schematically depicted by Figure 3.1. In the following,  $\beta \sim p$  denotes training labeling configurations drawn from the unknown underlying discrete joint data distribution  $p$ .  $\beta$  corresponds to the Dirac measure  $e_\beta \in \mathcal{S}_N$  (extreme point) of the meta-simplex  $\mathcal{S}_N$  and to a corresponding point  $\overline{W}_\beta = Me_\beta \in \overline{\mathcal{W}}$  to which the assignment flow (2.10) may converge.

The idea of flow matching is to directly fit the model vector field, in our case the assignment flow vector field (2.10),

$$V_\theta(W, t) := R_W[F_\theta(W, t)], \quad (3.7)$$

to a vector field whose flow realizes a desired measure transport. Let  $p_0 \in \mathcal{P}(\mathcal{W})$  be a simple reference measure and define conditional probability paths  $p_t(W|\beta)$  with the properties

$$p_0(W|\beta) := p_0(W) \quad (3.8a)$$

$$p_\infty(W|\beta) := \lim_{t \rightarrow \infty} p_t(W|\beta) = \delta_{\overline{W}_\beta}(W) \quad (3.8b)$$

for all  $\beta \in [c]^n$ . Then the marginal probability path

$$p_t(W) = \mathbb{E}_{\beta \sim p}[p_t(W|\beta)] \quad (3.9)$$

represents the target data distribution  $p$  in the limit  $t \rightarrow \infty$  by

$$p_\infty(W) := \lim_{t \rightarrow \infty} p_t(W), \quad \mathbb{E}_{W \sim p_\infty}[T(W)] = \mathbb{E}_{\beta \sim p}[e_\beta] = p. \quad (3.10)$$

In principle, we can now define a vector field  $u_t: \mathcal{W} \rightarrow \mathcal{T}$  which generates the path  $p_t$  in the sense that the flow of  $u_t$  pushes forward  $p_0$  to  $p_t$  for all times  $t \geq 0$ . Let  $\rho \in \mathcal{P}([0, \infty))$  be a distribution with full support on the non-negative time axis. Regression of the assignment flow vector field (3.7),  $V_\theta(\cdot, t): \mathcal{W} \rightarrow \mathcal{T}_0$ , with respect to  $u_t$ , amounts to minimizing the **Riemannian flow matching criterion**

$$\mathcal{L}_{\text{RFM}}(\theta) = \mathbb{E}_{t \sim \rho, W \sim p_t(W)} \left[ \|u_t(W) - V_\theta(W, t)\|_W^2 \right]. \quad (3.11)$$

In this form, flow matching is intractable, because we do not have access to the required field  $u_t$ . However, since we are at liberty to define conditional paths that are convenient within the constraints (3.8), we can choose  $p_t(\cdot|\beta)$  that are generated by conditional vector fields  $u_t(\cdot|\beta)$  with known form. The key insight in [CL23], based on [LCBH<sup>+</sup>23] and provided that each  $p_t(\cdot|\beta)$  is generated by  $u_t(\cdot|\beta)$ , is that the loss function (3.11) has the same gradient with respect to  $\theta$  as the **Riemannian conditional flow matching criterion**

$$\mathcal{L}_{\text{RCFM}}(\theta) = \mathbb{E}_{t \sim \rho, \beta \sim p, W \sim p_t(\cdot|\beta)} \left[ \|u_t(W|\beta) - V_\theta(W, t)\|_W^2 \right] \quad (3.12a)$$

$$\stackrel{(3.7)}{=} \mathbb{E}_{t \sim \rho, \beta \sim p, W \sim p_t(\cdot|\beta)} \left[ \|u_t(W|\beta) - R_W[F_\theta(W, t)]\|_W^2 \right]. \quad (3.12b)$$

By contrast to (3.11), conditional vector fields  $u_t(W|\beta)$  generating a path  $p_t(W|\beta)$  with the required properties (3.8) can be specified in closed form (cf. Proposition 3.17 below), and the conditional loss function (3.12) can be evaluated efficiently. Ultimately, by minimizing (3.12), the measure  $\nu_t$  generated from the reference measure  $\nu_0 = p_0$  by the assignment flow vector field  $R_W[F_\theta(W, t)]$  approximates  $p_\infty$  in the limit  $t \rightarrow \infty$ , which represents the unknown data distribution  $p$  through (3.10).

**3.3.2. Construction of Conditional Fields.** Let

$$\mathcal{N}_0(V) := \mathcal{N}(V; 0, \Pi_0) \quad (3.13)$$

denote the standard Gaussian centered in the tangent space at  $0 \in \mathcal{T}_0$ , with the orthogonal projection (2.8b) representing the identity map on  $\mathcal{T}_0 \subset \mathbb{R}^{n \times c}$ . Pushing forward  $\mathcal{N}_0$  by the lifting map (2.15) at the barycenter yields a simple *reference distribution*

$$p_0 = (\exp_{\mathbb{1}_{\mathcal{W}}})_{\#} \mathcal{N}_0 \in \mathcal{P}(\mathcal{W}). \quad (3.14)$$

The distribution (3.14) is simple in the sense that it is easy to draw samples and the conditions of Lemma 3.1 are satisfied; in particular,  $p_0$  factorizes node-wise. For each  $\beta \in [c]^n$  and a rate parameter  $\lambda > 0$ , define the probability path

$$t \mapsto \mathcal{N}_{t,\beta} := \mathcal{N}(\cdot; t\lambda V_\beta, \Pi_0) \in \mathcal{P}(\mathcal{T}), \quad V_\beta := \Pi_0 \overline{W}_\beta, \quad (3.15)$$

and lift it to  $\mathcal{W}$ , defining

$$p_t(\cdot|\beta) := (\exp_{\mathbb{1}_{\mathcal{W}}})_{\#} \mathcal{N}_{t,\beta}. \quad (3.16)$$

The parameter  $\lambda$  controls the *rate* at which  $p_t(\cdot|\beta)$  moves probability mass closer to  $\overline{W}_\beta$ . Small values of  $\lambda$  move the mass slowly; this is useful in settings with many labels  $c \gg 1$ , enabling the process to make class decisions during a longer time period. Figure 3.2 illustrates quantitatively the influence of  $\lambda$ .

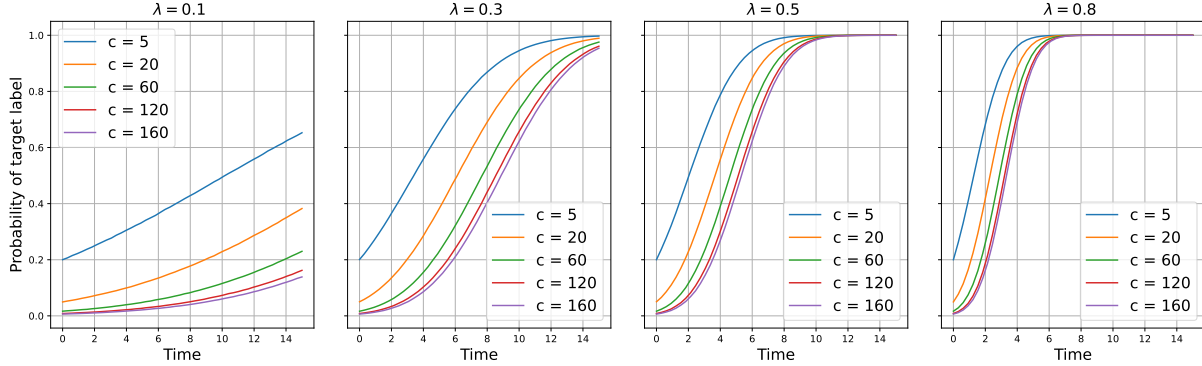


FIGURE 3.2. Influence of the parameter  $\lambda$  controlling in (3.15) and (3.19), respectively, the *rate* of assignment of mass of the pushforward probability measure (3.16) to a target label, depending on the number  $c$  of labels (classes, categories).

The following proposition makes explicit the conditional vector field that generates (3.16) and hence defines the training objective function (3.12). Recall the notation of Section 2.2 and the first paragraph of Section 3.3.1 explaining the one-to-one correspondence between a labelling configuration  $\beta$ , the corresponding Dirac measure  $e_\beta \in \mathcal{S}_N$  of the meta simplex, and the corresponding point  $\overline{W}_\beta \in \overline{W}$  of the closure of the assignment manifold.

**Proposition 3.2 (conditional vector fields).** *The probability paths defined in (3.16) are generated through the smooth flow*

$$\psi := \psi(\cdot|\overline{W}_\beta): \quad \mathbb{R}_{\geq 0} \times \mathcal{T}_0 \rightarrow \mathcal{W}, \quad (3.17a)$$

$$\psi_t(V) = \psi_t(V|\beta) = \exp_{\mathbb{1}_{\mathcal{W}}}(V + t\lambda V_\beta). \quad (3.17b)$$

*It is invertible and has the smooth inverse*

$$\psi_t^{-1}(W) := \psi_t^{-1}(W|\beta) = \exp_{\mathbb{1}_{\mathcal{W}}}^{-1}(W) - t\lambda V_\beta. \quad (3.18)$$

*In particular, the conditional vector field that generates (3.16) is given by*

$$u_t(W|\beta) = R_W[\lambda V_\beta]. \quad (3.19)$$

*Proof.* Since  $V_\beta$  does not depend on  $V$ , the map  $V \mapsto V + \lambda t V_\beta$  is affine. Hence, Eq. (3.17) conforms to (3.16), because affine transformations of normal distributions are again normal distributions. The mapping  $\exp_{\mathbb{1}_{\mathcal{W}}}(\cdot) : \mathcal{W} \rightarrow \mathcal{T}_0$  is a diffeomorphism. Consequently, the inverse of (3.17) can be computed from

$$W_t := \psi_t(V) = \exp_{\mathbb{1}_{\mathcal{W}}}(V + t\lambda V_\beta) \quad (3.20a)$$

$$\Leftrightarrow \psi_t^{-1}(W_t) = V = \exp_{\mathbb{1}_{\mathcal{W}}}^{-1}(W_t) - t\lambda V_\beta, \quad (3.20b)$$

which verifies (3.18). Recall that the conditional flow is determined by the conditional vector field through the ODE

$$\frac{d}{dt}\psi_t(V) = u_t(\psi_t(V)|\beta), \quad \psi_0(V) = \psi_0(V|\beta) = V. \quad (3.21)$$

Therefore the conditional vector field can be calculated using

$$u_t(W|\overline{W}_\beta) = \frac{d}{dt}\psi_t(\psi_t^{-1}(W)). \quad (3.22)$$

Computing the time derivative of the conditional flow

$$\frac{d}{dt}\psi_t(V) = R_{\psi_t(V)}[\lambda V_\beta], \quad (3.23)$$

and inserting (3.23) and (3.18) in (3.22) yields (3.19).  $\square$

**Proposition 3.3 (conditional path constraints).** *The conditional probability paths  $p_t(\cdot|\beta)$  defined by (3.16) satisfy the constraints (3.8).*

*Proof.* Equation (3.8a) is immediate due to (3.14) and (3.16). It remains to show that

$$\lim_{t \rightarrow \infty} p_t(\cdot|\beta) = \lim_{t \rightarrow \infty} (\psi_t)_\# p_0 = \delta_{\overline{W}_\beta}(\cdot). \quad (3.24)$$

To this end, we demonstrate that every marginal of the conditional probability path (3.24) converges to a Dirac measure supported on the assignment vector corresponding to the labeling configuration  $\beta$ , i.e.

$$\lim_{t \rightarrow \infty} p_{i;t}(\cdot|\beta) = \lim_{t \rightarrow \infty} (\psi_{t;i})_\# p_{0;i} = \delta_{\overline{W}_{\beta;i}}(\cdot), \quad i \in [n], \quad (3.25)$$

where  $p_{0;i}$ ,  $i \in [n]$  denote the marginals of  $p_0$  given by (3.14) and  $\psi_{t;i}(V_i) = \exp_{\mathbb{1}_S}(V_i + t\lambda V_{\beta;i})$  the marginal transformations (3.17).

First, we observe that by fixing an orthonormal basis  $\mathcal{B}$  of  $T_0$ , every marginal  $p_{0;i}$  of (3.14) with Gaussian  $\mathcal{N}_0$  defined by (3.13), can be expressed as the lifted image measure of a standard normal distribution  $\mathcal{N}(0_{c-1}, I_{c-1})$  on  $\mathbb{R}^{c-1}$  with respect to the basis  $\mathcal{B}$ ,

$$p_{0;i} = (\exp_{\mathbb{1}_S})_\# \mathcal{B}_\# \mathcal{N}(\cdot; 0_{c-1}, I_{c-1}) = (\exp_{\mathbb{1}_S})_\# \mathcal{N}(\cdot; 0_c, \pi_0), \quad (3.26)$$

since  $\mathcal{B}\mathcal{B}^\top = \pi_0$ . Consequently, by Proposition 3.2,

$$p_{i;t}(\cdot|\beta) = (\psi_{t;i})_\# \mathcal{N}(\cdot; 0_c, \pi_0) \quad (3.27)$$

and hence using the change-of-variables formula and (3.20b), for any  $S \in \mathcal{S}_c$ ,

$$p_{i;t}(S|\beta) = \mathcal{N}(\exp_{\mathbb{1}_S}^{-1}(S) - t\lambda V_{\beta;i}; 0_c, \pi_0) |\det d\psi_{t;i}^{-1}|. \quad (3.28)$$

Equation (3.18) shows that the differential  $d\psi_{t;i}^{-1}$  does not depend on  $t$ . Neither does the normalizing factor of the normal distribution, due to the covariance matrix  $\pi_0 = \text{id}_{T_0\mathcal{S}_c}$ . Consequently, since  $\psi_{t;i}^{-1}$  maps to  $T_0\mathcal{S}_c$ ,

$$p_{S;t}(S|\beta) \propto \exp\left(-\frac{1}{2}\langle \exp_{\mathbb{1}_S}^{-1}(S) - t\lambda V_{\beta;i}, \pi_0(\exp_{\mathbb{1}_S}^{-1}(S) - t\lambda V_{\beta;i}) \rangle\right) \quad (3.29a)$$

$$= \exp\left(-\frac{1}{2}\langle \exp_{\mathbb{1}_S}^{-1}(S) - t\lambda V_{\beta;i}, (\exp_{\mathbb{1}_S}^{-1}(S) - t\lambda V_{\beta;i}) \rangle\right) \rightarrow 0 \quad \text{as } t \rightarrow \infty, \quad (3.29b)$$

for any  $S \neq \overline{W}_{\beta;i} \in \overline{\mathcal{S}}_c$  and  $i \in [n]$ , due to the choice (3.15) of the tangent vector  $V_\beta$ . We conclude that the image measure  $p_{\infty;i}(\cdot|\beta)$  is a Dirac measure concentrated on  $\overline{W}_{\beta;i}$ .  $\square$

On  $\mathcal{T}$ , the path  $\mathcal{N}_t$  is generated by the constant vector field  $V \mapsto \lambda V_\beta$  given by (3.15). The related vector field on  $\mathcal{W}$ , which generates the path (3.16), is given by (3.19). Comparing the shape of this field to (2.10) makes clear that assignment flows are natural candidate dynamics for matching conditional paths of the described form. The Riemannian conditional flow matching objective (3.12) consequently reads

$$\mathcal{L}_{\text{RCFM}}(\theta) = \mathbb{E}_{t \sim \rho, \beta \sim p, W \sim p_t(\cdot|\beta)} \left[ \|R_W[\lambda V_\beta - F_\theta(W, t)]\|_W^2 \right]. \quad (3.30)$$

We point out that this criterion is ‘simulation free’, i.e. no integration of the assignment flow is required for loss evaluation, which makes training efficient.

Our approach (3.30) constitutes a novel instance of the flow-matching approach to generative modeling, introduced by [LCBH<sup>+</sup>23] and recently extended to Riemannian manifolds by [CL23]. This instance uses the assignment manifold (2.5a) and the corresponding Riemannian flow (2.10), along with the meta-simplex embedding (2.20), to devise a generative model whose underlying information geometry tailors the model to the representation and learning of *discrete joint* probability distributions.

**3.3.3. Infinite Integration Time.** A notable difference between our approach and previous Riemannian flow matching methods is that the target distribution is reached for  $t \rightarrow \infty$  rather than after finite time. This corresponds to the fact that  $e$ -geodesics do not reach boundary points of  $\overline{\mathcal{W}}$  after finite time and avoids two problems faced in prior work.

First, unlike the preliminary version presented in [BGAS24], data points  $\beta \in [c]^n$  do not need to be smoothed in order to present targets in the interior of  $\mathcal{W}$ . Instead, we can directly approach extreme points  $\overline{W}_\beta \in \overline{\mathcal{W}}$ , even though they are at infinity in the tangent space  $\mathcal{T}$  at  $\mathbb{1}_{\mathcal{W}}$ . Second, by not moving all mass of the reference distribution (close) to  $\overline{W}_\beta$  in finite time, we avoid a pathological behavior which can arise in flow matching on the simplex. Denote by

$$r_\beta = \left\{ W \in \mathcal{W} : \beta_i \in \arg \max_{j \in [c]} W_{i,j}, \forall i \in [n] \right\} \quad (3.31)$$

the subset of points in  $\mathcal{W}$  which assign their largest probability to the labels  $\beta$ . [SJW<sup>+</sup>24, Proposition 1] lays out that moving all mass of the reference distribution (close) to  $\overline{W}_\beta$  in *finite* time forces the model to make class decisions very early because the probability of  $r_\beta$  under  $p_t(\cdot|\beta)$  increases too quickly. The effect is exacerbated by increasing the number of classes  $c$  that the model is asked to discriminate between.

However, by opting for large integration time  $t \rightarrow \infty$  and a corresponding construction (3.16) of conditional probability paths, our approach is able to scale to many classes  $c \gg 1$ , avoiding the pathology described in [SJW<sup>+</sup>24, Proposition 1]. Formally, this is because  $p_t(\cdot|\beta)$  defined in (3.16) has full support on  $\mathcal{W}$  for every  $t \geq 0$ . In practice, the parameter  $\lambda$  in (3.15) can be used to control the speed at which the probability of  $r_\beta$  under  $p_t(\cdot|\beta)$  increases, allowing the model to make class decisions gradually over time.

Figure 4.5 (page 26) displays probability density paths for illustration. The corresponding impact on model accuracy is quantitatively shown in Figure 4.1 (page 22), with experimental details elaborated in Section 4.1.

**3.3.4. Relation to Dirichlet Flow Matching.** The construction of [SJW<sup>+</sup>24] specifically addresses pathological behavior of flow matching on the simplex, by choosing conditional probability paths  $p_t(\cdot|\beta)$  as paths of Dirichlet distributions. They demonstrate that this approach scales to at least  $c = 160$  classes, by allowing the model to make class decisions gradually over time. However, the explicit definition of  $p_t(\cdot|\beta)$  as paths of Dirichlet distributions makes it non-trivial to find corresponding vector fields  $u_t(\cdot|\beta)$  for flow matching, which leads them to make an ansatz for fields which move mass along straight lines in the ambient Euclidean space in which the probability simplex is embedded.

While we also make an explicit choice for  $p_t(\cdot|\beta)$  in (3.16), our construction is notably simpler than the approach of [SJW<sup>+</sup>24], allowing to easily compute the vector fields  $u_t(\cdot|\beta)$  by pushforward (Proposition 3.2). The resulting flow moves mass along  $e$ -geodesics on  $\mathcal{W}$ , which is much more natural with respect to the information geometry of discrete probability distributions. To illustrate this point, consider a straight path  $\hat{p}(t) \in \mathbb{R}^n$  with direction  $\frac{d}{dt}\hat{p}(t) = v \in \mathbb{R}^n$  at all times  $t$ . The trajectory  $\hat{p}(t)$  is generated by maximizing  $\langle v, \hat{p} \rangle$  along its gradient direction. On  $\mathcal{W}$ , the quantity  $\langle V_\beta, W \rangle$  can be interpreted as correlation between  $W \in \mathcal{W}$  and the direction  $V_\beta$ . The Riemannian gradient of this correlation with respect to the product Fisher-Rao geometry on  $\mathcal{W}$  is  $R_W[V_\beta]$ , i.e. precisely the direction of the conditional vector field (3.19).

**3.4. Learning Interaction between Simplices.** Our prior work [BCA<sup>+</sup>24] has studied the relationship between assignment flows on the product manifold  $\mathcal{W}$  and replicator dynamics on the meta-simplex  $\mathcal{S}_N$ . We now use core results of [BCA<sup>+</sup>24] to derive the flow matching approach of Section 3.3 from first principles of flow matching in  $\mathcal{S}_N$ . This demonstrates, in particular, that the proposed approach is suitable for *structured prediction* settings, in which multiple *coupled* random variables are of interest.

The result is surprising in the sense that direct flow matching of joint distributions in  $\mathcal{S}_N$  is intractable due to the combinatorial dimension  $N = c^n$ . However, by leveraging the special position of the submanifold  $\mathcal{T}$  (Figure 2.1) and compatibility of assignment flows with its geometry, we show that our construction can effectively break down combinatorial complexity and define a numerically tractable method.

The map  $T: \mathcal{W} \rightarrow \mathcal{S}_N$  defined in (2.20) associates a (marginal) distribution of  $n$  discrete random variables  $W \in \mathcal{W}$  with a factorizing joint distribution  $T(W) \in \mathcal{S}_N$ . Define with slight abuse of notation<sup>2</sup> the orthogonal projection

$$\pi_0: \mathbb{R}^N \rightarrow T_0\mathcal{S}_N \quad (3.32)$$

and formally denote the scaled standard normal distribution on  $T_0\mathcal{S}_N$  with variance  $c^{n-1}$  by

$$\mathcal{N}_0^{\mathcal{S}_N} = (\sqrt{c^{n-1}}\pi_0)_\# \mathcal{N}(0, \mathbb{1}_N) = \mathcal{N}(0, c^{n-1}\pi_0\pi_0^\top) = \mathcal{N}(0, c^{n-1}\pi_0). \quad (3.33)$$

Analogous to the construction of conditional measures in Section 3.3.2, we define the path of conditional measures

$$\mathcal{N}_t^{\mathcal{S}_N}(\cdot|\beta) = \mathcal{N}(\cdot; tc^{n-1}\lambda\pi_0e_\beta, c^{n-1}\pi_0) \quad (3.34)$$

given a labeling  $\beta \in [c]^n$  and a rate parameter  $\lambda > 0$ , scaled by the constant  $c^{n-1}$ . It follows from Proposition 3.3 that

$$p_t^{\mathcal{S}_N}(\cdot|\beta) = (\exp_{\mathbb{1}_{\mathcal{S}_N}})_\# \mathcal{N}_t^{\mathcal{S}_N}(\cdot|\beta) \quad (3.35)$$

satisfies the conditions (3.8) on  $\mathcal{S}_N$  and is thus suitable for flow matching on  $\mathcal{S}_N$  with reference distribution  $p_0 = \mathcal{N}_0^{\mathcal{S}_N}$ . Formally, the Riemannian conditional flow matching criterion analogous to (3.30) reads

$$\mathcal{L}_{\text{RCFM}}^{\mathcal{S}_N}(\theta) = \mathbb{E}_{t \sim \rho, \beta \sim p, q \sim p_t^{\mathcal{S}_N}(\cdot|\beta)} \left[ \left\| R_q[\lambda\pi_0e_\beta - f_\theta(q, t)] \right\|_w^2 \right] \quad (3.36)$$

for a payoff function  $f_\theta: \mathcal{S}_N \times [0, \infty) \rightarrow T_0\mathcal{S}_N$ . The task of minimizing (3.36) as written is numerically intractable, because we are not able to easily represent even general *points*  $q \in \mathcal{S}_N \setminus \mathcal{T}$  in the complement of the embedded assignment manifold  $\mathcal{T} = T(\mathcal{W})$  given by (2.20). To break down this complexity, we will define a projection onto  $\mathcal{T}$  by using the *lifting map lemma* [BCA<sup>+</sup>24, Lemma 3.3], which states

$$\exp_{\mathbb{1}_{\mathcal{S}_N}}(QV) = T(\exp_{\mathbb{1}_{\mathcal{W}}}(V)) \quad (3.37)$$

for all tangent vectors  $V \in T_0\mathcal{W}$ , with the mappings  $T$  and  $Q$  defined by (2.20) and (2.21). We start by an orthogonal projection  $T_0\mathcal{S}_N \rightarrow \text{img } Q \cap T_0\mathcal{S}_N$ .

**Lemma 3.4 (orthogonal projection onto  $\text{img } Q \cap T_0\mathcal{S}_N$ ).** *The orthogonal projection  $\text{proj}_0$  of tangent vectors in  $T_0\mathcal{S}_N$  to the subspace  $\text{img } Q \cap T_0\mathcal{S}_N$  reads*

$$\text{proj}_0: T_0\mathcal{S}_N \rightarrow \text{img } Q \cap T_0\mathcal{S}_N, \quad \text{proj}_0 v := Q_c \Pi_0 Q_c^\top v \quad \text{for } v \in T_0\mathcal{S}_N \quad (3.38)$$

in terms of the linear operator

$$Q_c := \frac{1}{\sqrt{c^{n-1}}} Q. \quad (3.39)$$

<sup>2</sup> $\pi_0$  is defined by (2.8a) as orthogonal projection onto the tangent space  $T_0\mathcal{S}_c$  of the *single* simplex  $\mathcal{S}_c$  with trivial tangent bundle  $\mathcal{S}_c \times T_0$ . Here, to simplify notation, we overload  $\pi_0$  to denote analogously the orthogonal projection onto the tangent space  $T_0\mathcal{S}_N$ .

*Proof.* By [BSS21, Lemma 4] we have  $Q^\top QV = c^{n-1}V$  for all  $V \in T_0\mathcal{W}$ . Thus,  $Q_c$  has the property

$$Q_c^\top Q_c V = V, \quad \text{for all } V \in T_0\mathcal{W}. \quad (3.40)$$

To show that (3.38) indeed defines orthogonal projection onto  $\text{img } Q \cap T_0\mathcal{S}_N$ , note that

$$Q_c \Pi_0 = \pi_0 Q_c \quad (3.41)$$

by [BCA<sup>+</sup>24, Lemma A.3] and accordingly

$$Q_c^\top \pi_0 = (\pi_0 Q_c)^\top = (Q_c \Pi_0)^\top = \Pi_0 Q_c^\top \quad (3.42)$$

by using the symmetry of  $\Pi_0$  and  $\pi_0$ . We can use this to show  $\text{img } \text{proj}_0 \subseteq \text{img } Q \cap T_0\mathcal{S}_N$  because for any  $x \in \mathbb{R}^{n \times c}$ , we have

$$Q_c \Pi_0 x \in \text{img } Q \quad \text{and} \quad Q_c \Pi_0 x \stackrel{(3.41)}{=} \pi_0 Q_c x \in T_0\mathcal{S}_N. \quad (3.43)$$

Now let  $v \in T_0\mathcal{S}_N$  and  $y \in \text{img } Q \cap T_0\mathcal{S}_N$  be arbitrary. Then  $y$  can be written as  $y = Q_c y'$  and we have

$$\langle v - \text{proj}_0 v, y \rangle = \langle v - Q_c \Pi_0 Q_c^\top v, Q_c y' \rangle = \langle Q_c^\top v - Q_c^\top Q_c \Pi_0 Q_c^\top v, y' \rangle \quad (3.44a)$$

$$\stackrel{(3.40)}{=} \langle Q_c^\top v - \Pi_0 Q_c^\top v, y' \rangle \stackrel{(3.42)}{=} \langle Q_c^\top v - Q_c^\top \pi_0 v, y' \rangle \quad (3.44b)$$

$$= 0, \quad (3.44c)$$

which shows that  $\text{proj}_0$  projects orthogonally.  $\square$

Since (3.37) ensures that  $\exp_{\mathbb{1}_{\mathcal{S}_N}}(\text{img } Q) \subseteq \mathcal{T}$ , we can now define the projection

$$\text{proj}_{\mathcal{T}} := \exp_{\mathbb{1}_{\mathcal{S}_N}} \circ \text{proj}_0 \circ \exp_{\mathbb{1}_{\mathcal{S}_N}}^{-1} : \mathcal{S}_N \rightarrow \mathcal{T}. \quad (3.45)$$

Under this projection, the conditional measures  $p_t^{\mathcal{S}_N}(\cdot|\beta) \in \mathcal{P}(\mathcal{S}_N)$  precisely induce the conditional probability paths  $p_t(\cdot|\beta) \in \mathcal{P}(\mathcal{W})$  defined in (3.16). Note that every extreme point of  $\mathcal{S}_N$  lies in (the closure of)  $\mathcal{T}$ . Thus, projecting to  $\mathcal{T}$  preserves the endpoints  $\delta_{e_\beta}$  reached by the conditional distributions (3.35) in the limit  $t \rightarrow \infty$ . In particular, the projection transforms the intractable conditional flow matching criterion (3.36) on  $\mathcal{S}_N$  into the numerically tractable criterion (3.30).

**Theorem 3.5 (projected flow matching on  $\mathcal{S}_N$ ).** *For any  $\beta \in [c]^n$ , the pushforward of the conditional measure  $p_t^{\mathcal{S}_N}(\cdot|\beta)$  defined in (3.35) under the projection  $\text{proj}_{\mathcal{T}} : \mathcal{S}_N \rightarrow \mathcal{T}$  defined in (3.45) is*

$$(\text{proj}_{\mathcal{T}})_\# p_t^{\mathcal{S}_N}(\cdot|\beta) = T_\# p_t(\cdot|\beta) \quad (3.46)$$

with  $p_t(\cdot|\beta) \in \mathcal{P}(\mathcal{W})$  defined in (3.16) and the embedding map  $T$  given by (2.20). Furthermore, the flow matching criterion on  $\mathcal{T}$ , induced by the conditional paths (3.46), reads

$$\mathcal{L}_{\text{RCFM}}^{\mathcal{T}}(\theta) = \mathbb{E}_{t \sim \rho, \beta \sim p, q \sim (\text{proj}_{\mathcal{T}})_\# p_t^{\mathcal{S}_N}(\cdot|\beta)} \left[ \left\| R_q[\lambda \pi_0 e_\beta - \tilde{f}_\theta(q, t)] \right\|_w^2 \right] \quad (3.47)$$

and, using the ansatz  $\tilde{f}_\theta = Q \circ F_\theta \circ M$  with  $Q$  and  $M$  defined by (2.21) and (2.23b), (3.47) is equal to the criterion (3.30) for flow matching assignment flows on  $\mathcal{W}$ .

*Proof.* We use the representation of  $\text{proj}_0$  (Lemma 3.4) to compute the pushforward (3.46).

$$(\text{proj}_{\mathcal{T}})_{\#} p_t^{S_N}(\cdot|\beta) \stackrel{(3.45)}{=} (\exp_{\mathbb{1}_{S_N}} \circ \text{proj}_0 \circ \exp_{\mathbb{1}_{S_N}}^{-1})_{\#} p_t^{S_N}(\cdot|\beta) \quad (3.48a)$$

$$\stackrel{(3.35)}{=} (\exp_{\mathbb{1}_{S_N}} \circ \text{proj}_0)_{\#} \mathcal{N}_t^{S_N}(\cdot|\beta) \quad (3.48b)$$

$$\stackrel{(3.38)}{=} (\exp_{\mathbb{1}_{S_N}} \circ Q_c \Pi_0 Q_c^{\top})_{\#} \mathcal{N}_t^{S_N}(\cdot|\beta) \quad (3.48c)$$

$$\stackrel{(3.34)}{=} (\exp_{\mathbb{1}_{S_N}} \circ Q_c \Pi_0 Q_c^{\top})_{\#} \mathcal{N}(\cdot; t c^{n-1} \lambda \pi_0 e_{\beta}, c^{n-1} \pi_0) \quad (3.48d)$$

$$= (\exp_{\mathbb{1}_{S_N}})_{\#} \mathcal{N}(\cdot; t c^{n-1} \lambda Q_c \Pi_0 Q_c^{\top} \pi_0 e_{\beta}, c^{n-1} Q_c \Pi_0 Q_c^{\top} \pi_0 (Q_c \Pi_0 Q_c^{\top})^{\top}) \quad (3.48e)$$

$$\stackrel{(3.39)}{=} \stackrel{(3.42)}{=} (\exp_{\mathbb{1}_{S_N}})_{\#} \mathcal{N}(\cdot; t \lambda Q \Pi_0 Q^{\top} e_{\beta}, c^{n-1} Q_c \Pi_0 Q_c^{\top} Q_c \Pi_0 Q_c^{\top}) \quad (3.48f)$$

$$\stackrel{(3.39)}{=} \stackrel{(3.40)}{=} (\exp_{\mathbb{1}_{S_N}})_{\#} \mathcal{N}(\cdot; t \lambda Q \Pi_0 Q^{\top} e_{\beta}, Q \Pi_0 Q^{\top}) \quad (3.48g)$$

$$= (\exp_{\mathbb{1}_{S_N}} \circ Q)_{\#} \mathcal{N}(\cdot; t \lambda \Pi_0 Q^{\top} e_{\beta}, \Pi_0). \quad (3.48h)$$

By [BCA<sup>+</sup>24, Lemma 3.4], we have  $Q^{\top} e_{\beta} = M e_{\beta}$ . Using the shorthand  $V_{\beta}$  defined in (3.15) and the lifting map lemma (3.37), this shows

$$(\text{proj}_{\mathcal{T}})_{\#} p_t^{S_N}(\cdot|\beta) = (\exp_{\mathbb{1}_{S_N}} \circ Q)_{\#} \mathcal{N}(\cdot; t \lambda V_{\beta}, \Pi_0) \quad (3.49a)$$

$$\stackrel{(3.37)}{=} (T \circ \exp_{\mathbb{1}_{\mathcal{W}}})_{\#} \mathcal{N}(\cdot; t \lambda V_{\beta}, \Pi_0) \quad (3.49b)$$

$$\stackrel{(3.15)}{=} (T \circ \exp_{\mathbb{1}_{\mathcal{W}}})_{\#} \mathcal{N}_{t,\beta} \quad (3.49c)$$

$$\stackrel{(3.16)}{=} T_{\#} p_t(\cdot|\beta) \quad (3.49d)$$

which is the assertion (3.46).

Returning to (3.49a), we can compute the conditional vector field whose flow produces the path  $(\text{proj}_{\mathcal{T}})_{\#} p_t^{S_N}(\cdot|\beta)$  by

$$u_t^{\mathcal{T}}(q|\beta) = d \exp_{\mathbb{1}_{S_N}}(v) [\lambda Q V_{\beta}] = R_q [\lambda Q V_{\beta}] \quad (3.50)$$

with  $v = \exp_{\mathbb{1}_{S_N}}^{-1}(q)$  analogous to (3.19). This shows the shape of the flow matching criterion (3.47). It remains to show that it is equal to (3.30).

Substituting the ansatz  $f_{\theta} = Q \circ F_{\theta} \circ M$  into this criterion gives

$$\mathcal{L}_{\text{RCFM}}^{\mathcal{T}} = \mathbb{E}_{t \sim \rho, \beta \sim p, W \sim p_t(\cdot|\beta)} \left[ \left\| R_{T(W)} [\lambda Q (V_{\beta}) - (Q \circ F_{\theta})(W, t)] \right\|_{T(W)}^2 \right]. \quad (3.51)$$

By [BCA<sup>+</sup>24, Theorem 3.1],  $T: \mathcal{W} \rightarrow \mathcal{T} \subseteq \mathcal{S}_N$  defined by (2.20) is a Riemannian isometry. Thus, for any vector field  $X: \mathcal{W} \rightarrow \mathcal{T}$  and any  $W \in \mathcal{W}$ , it holds that

$$\langle R_W[X], R_W[X] \rangle_W = \langle dT_W[R_W[X]], dT_W[R_W[X]] \rangle_{T(W)}. \quad (3.52)$$

Furthermore, by [BCA<sup>+</sup>24, Theorem 3.5], one has

$$dT_W[R_W[X]] = R_{T(W)}[QX]. \quad (3.53)$$

Taking (3.52) and (3.53) together, (3.51) transforms to

$$\mathcal{L}_{\text{RCFM}}^{\mathcal{T}} = \mathbb{E}_{t \sim \rho, \beta \sim p, W \sim p_t(\cdot|\beta)} \left[ \left\| R_W[\lambda V_{\beta} - F_{\theta}(W, t)] \right\|_W^2 \right] \quad (3.54)$$

which is (3.30).  $\square$

Theorem 3.5 shows that the constructed flow matching on  $\mathcal{W}$ , which operates separately on multiple simplices, is induced by flow matching in the *single* meta-simplex  $\mathcal{S}_N$ , with conditional distribution paths and vector fields projected to the submanifold  $\mathcal{T} = T(\mathcal{W})$ . This result provides a geometric justification for the fact that interaction between simplices is learned through flow matching, even though all conditional probability paths  $p_t(\cdot|\beta)$  used in training can be separately constructed on individual simplices.

**3.5. Numerical Flow Integration.** We point out again that learning our generative model by Riemannian flow matching is ‘simulation free’: numerical integration is not required since only vector fields have to be matched which are defined on the tangent bundle of the assignment manifold and on the corresponding tangent-subspace distribution of the meta simplex (Prop. 3.5), respectively. On the other hand, numerical integration of the flow is required for evaluating the learned generative model, in order to sample as illustrated by Figure 1.1, or for likelihood computation (Section 3.6).

Since the flow corresponds to an ODE on a Riemannian manifold, *geometric* numerical integration utilizes various representations of the ODE on the tangent bundle in order to apply established methods for numerical integration on Euclidean spaces [HLW06]. In the case of the assignment flow, this has been thoroughly studied by [ZSPS20] using the extension of the lifting map (2.15) to the product manifold (2.5), regarded as action of the respective tangent space (regarded as additive abelian Lie group) on the assignment manifold. From the general viewpoint of geometric numerical integration, the resulting schemes for geometric numerical integration categorize as Runge-Kutta schemes of Munthe-Kaas type [MK99].

Specifically, in this paper, numerical integration was carried out using the classical explicit embedded Dormand & Prince Runge-Kutta method [DP80] of orders 4 & 5 with stepsize control (cf. [ZSPS20, Section 5.2] and [HNW08, Section II.5]).

**3.6. Likelihood Computation.** The likelihood of test data under the model distribution  $\tilde{p}$  is commonly used as a surrogate for Kullback-Leibler divergence between  $\tilde{p}$  and the true data distribution  $p$ , due to the relationship

$$\text{KL}(p, \tilde{p}) = \mathbb{E}_p \left[ \log \frac{p}{\tilde{p}} \right] = -H(p) - \mathbb{E}_p[\log \tilde{p}]. \quad (3.55)$$

The entropy  $H(p)$  is a property of the data distribution, which is not typically known, but can be treated as a constant which does not depend on the model. For continuous normalizing flows, likelihood under the model is directly used as a training criterion for this reason. Using the instantaneous change-of-variables formula [CRBD18]

$$\frac{\partial}{\partial t} \log \nu_t(x) = -\text{tr} J(x, t), \quad (3.56)$$

log-likelihood under continuous normalizing flows can, on continuous state spaces, be computed by integrating (3.56) backward in time. In (3.56),  $J(x, t)$  denotes the vector field Jacobian, whose trace is commonly approximated by using Hutchinson’s estimator [Hut89]

$$\text{tr} J = \mathbb{E}_v[\langle v, Jv \rangle] \quad (3.57)$$

with  $v$  drawn from a fixed normal or Rademacher distribution. The use of this estimator in the context of likelihood under continuous normalizing flows was proposed by [GCB<sup>+</sup>19]. The authors use a single sample  $v$  for each integration of (3.56), which yields an unbiased estimator for log-likelihood of independent test data. In order to use likelihood as a training criterion, numerical integration of (3.56) is required. This entails many forward and backward passes through the employed network architecture in order to compute a single parameter update.

Therefore, we do not use likelihood as a training criterion, opting instead for the simulation-free flow matching approach of Section 3.3. Since the learned model is still a normalizing flow, (3.56) remains a useful tool for computing likelihoods under our model. However, because we are modeling discrete data

while working on continuous state spaces, likelihood of discrete data can not be computed as a point estimate on  $\mathcal{W}$ . Further details are provided in Appendix B.

**3.7. Dequantization.** Approximation of discrete data distributions by continuous distributions has been studied through the lens of *dequantization*. Choose a latent space  $\mathcal{F}^n$  and an embedding of class label configurations  $\beta \in [c]^n$  as prototypical points  $f_\beta^* \in \mathcal{F}^n$ . Suppose the choice of these points is fixed before training and associate disjoint sets  $A_\beta \subseteq \mathcal{F}^n$  with label configurations such that they form a partition of  $\mathcal{F}^n$  and  $f_\beta^* \in A_\beta$ . We can then define the continuous surrogate model

$$\vartheta = \sum_{\beta \in [c]^n} p_\beta \mathcal{U}_{A_\beta} \in \mathcal{P}(\mathcal{F}^n) \quad (3.58)$$

which represents  $p \in \mathcal{S}_N$  as a mixture of uniform distributions  $\mathcal{U}_{A_\beta}$ , supported on the disjoint subsets  $A_\beta$ . The underlying idea is that

$$\mathbb{P}_\vartheta(A_\beta) = \int_{A_\beta} \vartheta(y) dy = p_\beta \int_{A_\beta} \mathcal{U}_{A_\beta}(y) dy = p_\beta \quad (3.59)$$

due to the disjoint support of mixture components in (3.58). Denote a continuous model distribution by  $\nu \in \mathcal{P}(\mathcal{F}^n)$ . Using Jensen's inequality, we find

$$-H(\vartheta) - \text{KL}(\vartheta, \nu) = \int \vartheta(y) \log \nu(y) dy = \sum_{\beta \in [c]^n} p_\beta \int_{A_\beta} \log \nu(y) dy \quad (3.60a)$$

$$\leq \sum_{\beta \in [c]^n} p_\beta \log \int_{A_\beta} \nu(y) dy \quad (3.60b)$$

$$= -H(p) - \text{KL}(p, q) \quad (3.60c)$$

for the discrete model distribution  $q$  defined by

$$q_\beta = \int_{A_\beta} \nu(y) dy = \mathbb{P}_\nu(A_\beta). \quad (3.61)$$

Thus, fitting  $\nu$  to  $\vartheta$  by maximizing log-likelihood of smoothed data drawn from  $\vartheta$  implicitly minimizes an upper bound on the relative entropy  $\text{KL}(p, q)$ . In practice, drawing smoothed data from  $\vartheta$  amounts to adding noise to the prototypes  $f_{\beta_k}^* \in \mathcal{F}^n$  of discrete data  $\{\beta_k\}_{k \in [m]}$ .

The above *dequantization approach* was first proposed by [TvdOB16]. Their reasoning justifies the previously known heuristic of adding noise to dequantize data [UML13]. It has thenceforth become common practice for training normalizing flows as generative models of images [DSDB17, SKCK17] and was generalized to non-uniform noise distributions by [HCS<sup>+</sup>19]. These authors focus on image data which, although originally continuous, are only available discretized into 8-bit integer color values for efficient digital storage. In this case, the underlying continuous color imparts a natural structure on the set of discrete classes. Similar colors are naturally represented as prototypes which are close to each other with respect to some metric on the feature space  $\mathcal{F}^n$ .

For the *general* discrete data considered here, such a structure is not available. As a remedy, [CAN22] present an approach to learn the embedding jointly with likelihood maximization and defining the partition of  $\mathcal{F}^n$  into subsets  $A_\beta$  through Voronoi tessellation. The rounding model variant (B.1) of our approach can be seen as dequantization on the space  $\mathcal{F}^n = \mathcal{W}$  with prototypical points  $f_\beta^* = \overline{W}_\beta$ . The sets  $A_\beta$  generated by Voronoi tessellation then coincide with the sets  $r_\beta$  defined by (3.31). However, our approach differs from [CAN22] by using flow matching instead of likelihood-based training and by explicit consideration of information geometry on  $\mathcal{W}$ .

A natural question is whether the ability to learn an embedding of class configurations as prototypical points  $f_\beta^*$ , thereby representing similarity relations between classes, can be replicated in our setting. Indeed, because points in  $\mathcal{S}_c$  have a clear interpretation as categorical distributions, it is easy to achieve this goal by extending the payoff function  $F_\theta$  of the assignment flow (2.10).

For some  $L > 0$ , let  $E \in \mathbb{R}^{L \times c}$  be a learnable embedding matrix. The columns of  $E$  can be seen as prototypical points in the Euclidean latent space  $\mathbb{R}^L$ . The action of  $E$  on an integer probability vector  $e_j \in \mathcal{S}_c$  precisely selects one of these points, associating it with the class  $j \in [c]$ . Learning  $E$  now allows to represent relationships between classes in the latent space  $\mathbb{R}^L$ . Let  $\mathcal{E}: \mathbb{R}^{n \times c} \rightarrow \mathbb{R}^{n \times c}$  denote the linear operator which applies  $E$  nodewise. We now choose a parameterized function  $\tilde{F}_\theta: \mathbb{R}^L \rightarrow \mathbb{R}^L$  that operates on  $\mathbb{R}^L$  and define the extended payoff function

$$F_\theta = \mathcal{E}^\top \circ \tilde{F}_\theta \circ \mathcal{E}: \mathcal{W} \rightarrow \mathbb{R}^{n \times c}. \quad (3.62)$$

#### 4. EXPERIMENTS AND DISCUSSION

As outlined in Section 3, we perform Riemannian flow-matching (3.11) via the conditional objective (3.30) to learn assignment flows (2.10). These in turn approximate  $p_\infty$  in the limit  $t \rightarrow \infty$  and thereby the unknown data distribution  $p$  through (3.10).

**4.1. Class Scaling.** First, we replicate the experiment of [SJW<sup>+</sup>24, Figure 4] to verify that our model is able to make decisions gradually over longer integration time and can scale to many classes  $c$ . Details of the training procedure are relegated to Appendix A.1. For each  $c$ , the data distribution is a randomly generated, factorizing distribution on  $n = 4$  simplices.

Figure 4.1 shows the relative entropy between the learned models (histogram of 512k samples) and the known target distribution. Our proposed approach is able to outperform our earlier method [BGAS24] (green) as well as Dirichlet flow matching [SJW<sup>+</sup>24] (orange) and the linear flow matching baseline (blue) in terms of scaling to many classes  $c$ . In Figure 4.1, the linear flow matching baseline scales better to many classes than in [SJW<sup>+</sup>24, Figure 4], but the qualitative statement that linear flow matching is ill-suited to this end is still supported by our empirical findings. Our preliminary approach [BGAS24] (green) also scales comparatively well, even outperforming Dirichlet flow matching. Figures 4.5 and 4.6 illustrate probability paths  $p_t(\cdot|\beta)$  for our approach (cf. (3.16)) and Dirichlet flow matching [SJW<sup>+</sup>24] at different time scales.

A property of assignment flow approaches, possibly linked to observed performance, is to transport probability mass relative to the underlying Fisher Rao geometry (recall Section 3.3.4). For example, this leads to little probability mass in regions close to the simplex boundaries (Figure 4.5).

**4.2. Generating Image Segmentations.** In image segmentation, a joint assignment of classes to pixels is usually sought conditioned on the pixel values themselves. Here, we instead focus on the *unconditional* discrete distribution of segmentations, without regard to the original pixel data. These discrete distributions are very high-dimensional in general, with  $N = c^n$  increasing exponentially in the number of pixels.

To this end, we parametrize  $F_\theta$  by the UNet architecture of [DN21] and train on downsampled segmentations of Cityscapes [COR<sup>+</sup>16] images, as well as MNIST [LCB10], regarded as binary  $c = 2$  segmentations after thresholding continuous pixel values at 0.5. Details of the training procedure are relegated to Appendix A.2.

Figures 4.2 and 4.3 show samples from the learned distribution of binarized MNIST and Cityscapes segmentations respectively, next to the closest training data. This illustrates that our model is able to interpolate the data distribution, without simply memorizing training data. Additional samples from our Cityscapes model are shown in Figure 4.4.

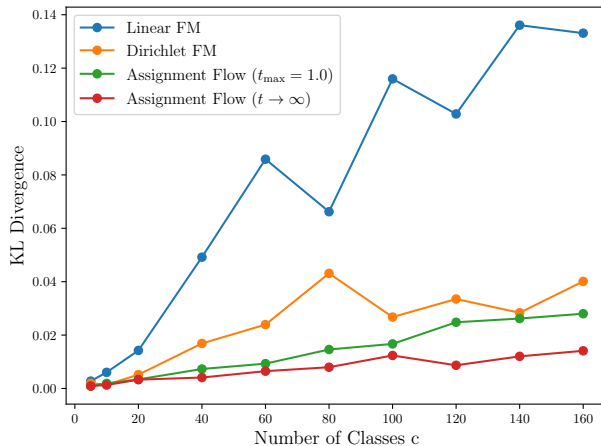


FIGURE 4.1. Relative entropy between learned models (histogram of 512k samples) and a known, factorizing target distribution on  $n = 4$  simplices with varying number of classes  $c$ . By leveraging information geometry and gradual decision-making over time, our proposed approach (red) is able to outperform our earlier method [BGAS24] as well as Dirichlet flow matching [SJW<sup>+</sup>24] in terms of scaling to many classes  $c$ .

**4.3. Likelihood Evaluation.** We compute the likelihood of test data from the MNIST dataset (binarized by thresholding) using the method described in Section 3.6. We use 100 priority samples per datum and, as is common practice for normalizing flows, only a single Hutchinson sample. The result is shown in Table 1, compared to our earlier approach [BGAS24] ( $t \rightarrow 1$ ). For comparison, we show likelihood of MNIST test data (from the *continuous*, non-binarized distribution) under several normalizing flow methods from the literature which were trained using likelihood maximization.

Note that, although much prior work on generative modelling has been applied to continuous gray value MNIST images, binarization (in our case through thresholding) substantially changes the data distribution. Thus, likelihood of test data, which is commonly used as a surrogate for relative entropy to the data distribution in normalizing flows, is not comparable between these methods and ours. In addition, since we do not use likelihood maximization as a training criterion, it is not to be expected that our model is competitive on this measure. Still, the results of Table 1 indicate that the proposed model ( $t \rightarrow \infty$ ) fits the binarized MNIST data distribution better in terms of relative entropy than our previous approach [BGAS24] ( $t \rightarrow 1$ ).

TABLE 1. Likelihood of binarized MNIST test data under our proposed model ( $t \rightarrow \infty$ ) and the earlier version [BGAS24] ( $t \rightarrow 1$ ). Both methods are trained by flow matching rather than likelihood maximization.

Method	AF ( $t \rightarrow \infty$ )	AF ( $t \rightarrow 1$ )
Likelihood (bits / dim)	$1.01 \pm 0.17$	$4.05 \pm 0.83$

## 5. CONCLUSION

We introduced a novel generative model for the representation and evaluation of joint probability distributions of discrete random variables. The approach employs an embedding of the assignment manifold in the meta-simplex of all joint probability distributions. Corresponding measure transport by randomized assignment flows approximates joint distributions of discrete random variables in a principled manner. The approach enables to learn the statistical dependencies of any set of discrete random variables, and using the resulting model for structured prediction, independent of the area of application.

Inference using the approach is computationally efficient, since sampling can be accomplished by parallel geometric numerical integration. Training the generative model using given empirical data is computationally efficient, since matching the flow of corresponding e-geodesics is used as training criterion, which does not require sampling as a subroutine.

Numerical experiments showed superior performance in comparison to recent related work, which we attribute to consistently using the underlying information geometry of assignment flows and the corresponding measure transport along conditional probability paths. On the other hand, the fact that even our *preliminary* approach [BGAS24] can outperform Dirichlet flow matching [SJW<sup>+</sup>24] with respect to scaling to many classes in Figure 4.1, is surprising, because the approach [BGAS24] uses a *finite* integration time and moves all mass of the reference distribution to a Dirac measure close to  $\bar{W}_\beta$  within this finite time. The core assumptions of [SJW<sup>+</sup>24, Proposition 1], therefore, apply to this approach, and the fact that it still performs well empirically suggests that further inquiry into this topic is warranted.

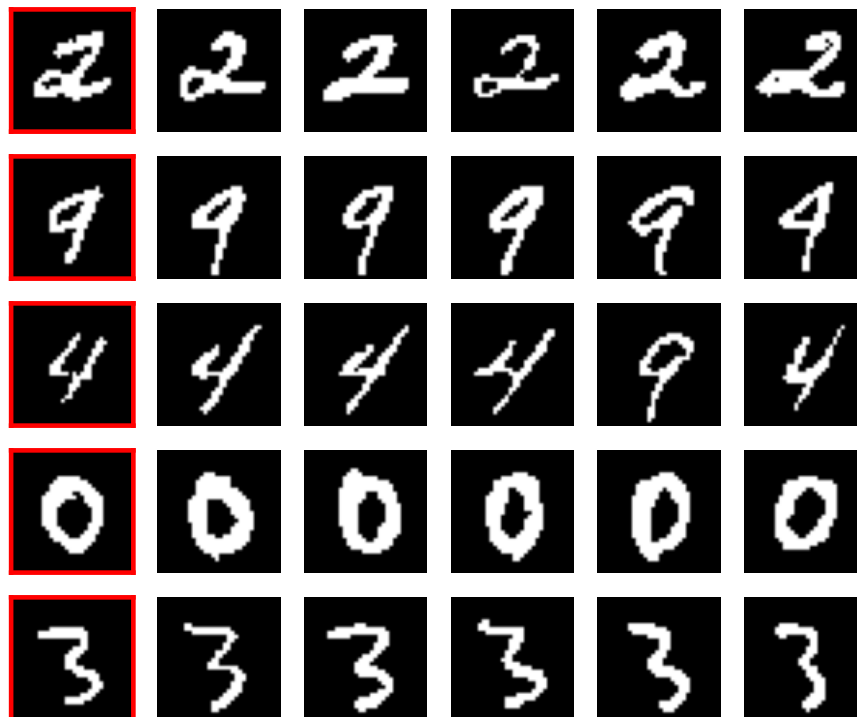


FIGURE 4.2. Comparison of model samples to the closest training data. *Left with red border*: samples drawn from our model of the binarized MNIST distribution. *Right*: training data closest to the sample in terms of pixel-wise distance.

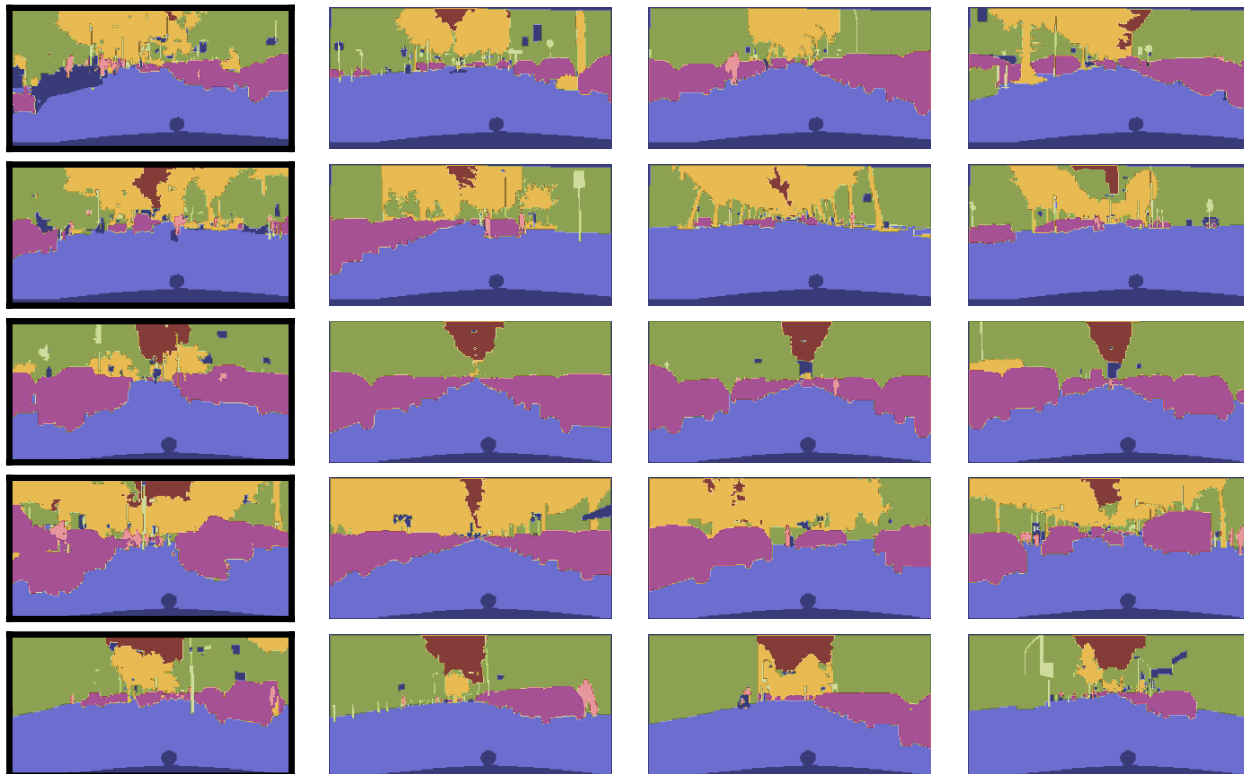


FIGURE 4.3. Comparison of model samples to the closest training data. *Left with black border*: samples drawn from our model of the Cityscapes segmentation distribution. *Right*: training data closest to the sample in terms of pixel-wise distance.

## APPENDIX A. EXPERIMENTS: DETAILS

**A.1. Details of Class Scaling Experiment.** To parameterize  $F_\theta$ , we use the same convolutional architecture used in [SJW<sup>+</sup>24]. We train for 500k steps of the Adam optimizer with constant learning rate  $3 \cdot 10^{-4}$  and batch size 128. We reproduce the Dirichlet flow matching results and linear flow matching baseline by using the code of [SJW<sup>+</sup>24]. The experiment shown in Figure 4.1 is slightly harder than the version in [SJW<sup>+</sup>24], because we limit training to 64k steps at batch size 512 for Dirichlet- and linear flow matching. Accordingly, both assignment flow methods are trained for 250k steps at batch size 128, such that around 32M data are seen by each model during training.

### A.2. Details of generating Image Segmentation.

**A.2.1. Cityscapes Data Preparation.** Rather than the original  $c = 33$  classes, we only use the  $c = 8$  classes specified as *categories* in *torchvision*. The same subsampling of classes was used in the related work [HNJ<sup>+</sup>21]. They additionally perform spatial subsampling to  $32 \times 64$ . Instead, we subsample the spatial dimensions (*NEAREST* interpolation) to  $128 \times 256$ .

**A.2.2. Cityscapes Training.** For the Cityscapes experiment, we employ the UNet architecture of [DN21] with *attention\_resolutions* (32, 16, 8), *channel\_mult* (1,1,2,3,4), 4 attention heads, 3 blocks and 64 channels. We trained for 250 epochs using Adam with cosine annealing learning rate scheduler starting at learning rate 0.0003 and batch size 4. The distribution  $\rho$  of times  $t$  used during training is an exponential distribution with rate parameter  $\lambda = 0.25$ . For sampling, we integrate up to  $t_{\max} = 15$ .

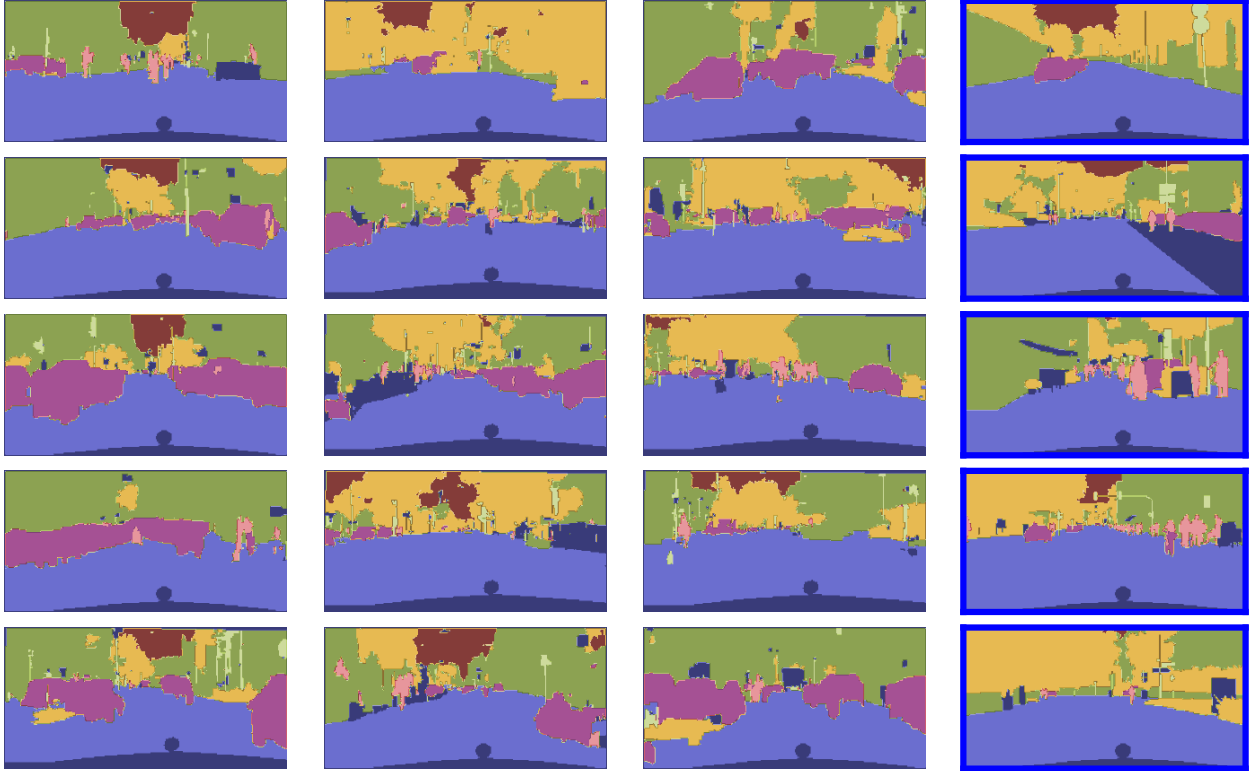


FIGURE 4.4. *Left*: Samples from our model of the Cityscapes segmentation distribution. *Right with blue border*: randomly drawn training data.

A.2.3. *Binarized MNIST Data Preparation.* We pad the original  $28 \times 28$  images with zeros to size  $32 \times 32$  to be compatible with spatial downsampling employed by the UNet architecture. Binarization is performed by pixelwise thresholding at grayvalue 0.5.

A.2.4. *Binarized MNIST Training.* We modify the same architecture used for Cityscapes to *attention\_resolutions* (16), *channel\_mult* (1,2,2,2), 4 attention heads, 2 blocks and 32 channels. The same training regimen is used as for Cityscapes except for an increase in batch size to 256. The distribution  $\rho$  of times  $t$  used during training is an exponential distribution with rate parameter  $\lambda = 0.5$ . For sampling, we integrate up to  $t_{\max} = 10$ . In table 1, we use the same UNet architecture and training regimen for the comparison method [BGAS24] ( $t \rightarrow 1$ ).

## APPENDIX B. LIKELIHOOD COMPUTATION: DETAILS

Assume we have learned a probability path  $\nu_t$  and a final pushforward distribution  $\nu_\infty$ . In practice, numerical integration needs to be stopped after a finite time  $t = t_{\max}$ , reaching a numerical pushforward distribution  $\nu_{t_{\max}} \approx \nu_\infty$ . Drawing samples from  $\tilde{p} = \mathbb{E}_{W \sim \nu_{t_{\max}}} [T(W)]$  is a two-stage process:  $W \sim \nu_{t_{\max}}$  is drawn first, followed by sampling  $\beta \sim T(W)$ . Due to the numerical need to stop integration at finite time,  $T(W)$  may in practice not have fully reached a discrete Dirac distribution. For long sequences of random variables, such as text or image modalities, this can lead to undesirable noise in the output samples. A way to combat this numerical problem is by rounding to a Dirac measure before sampling. This procedure can be interpreted within the framework of *dequantization*, which we elaborate in Section 3.7.

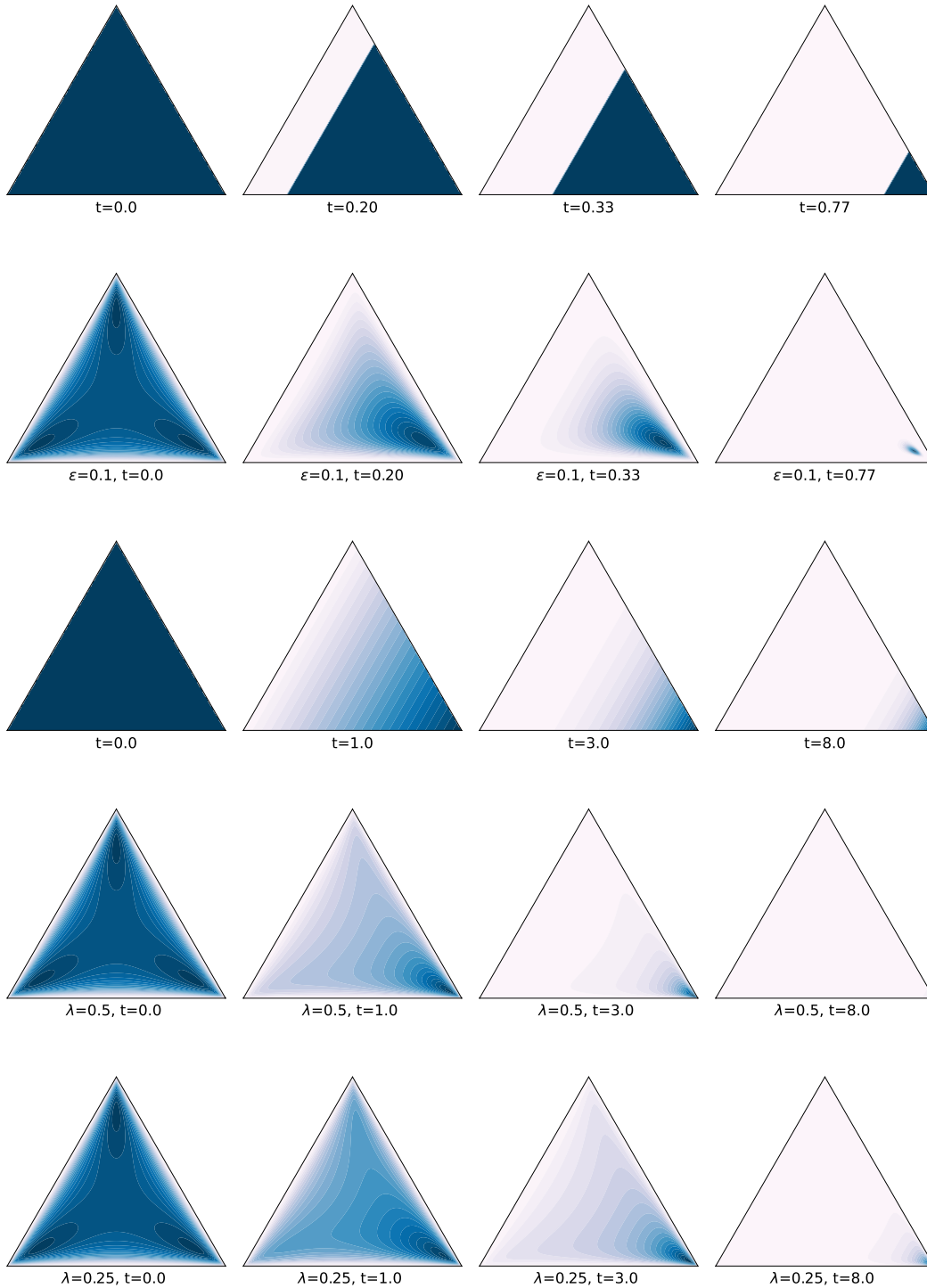


FIGURE 4.5. Plots of conditional densities  $p_t(\cdot|\beta)$  for different points of time  $t$ . Darker colors indicate higher concentration within the densities. *From top to bottom*: Linear Flow Matching [SJW<sup>+</sup>24, Equation 11], the approach [BGAS24, Equation 18], Dirichlet Flow Matching [SJW<sup>+</sup>24, Equation 14], our approach (3.16) using two different values of the rate parameter  $\lambda$ . Note the different time periods  $t \in [0, 0.77]$  used for the first two and  $t \in [0, 8]$  for the latter approaches.

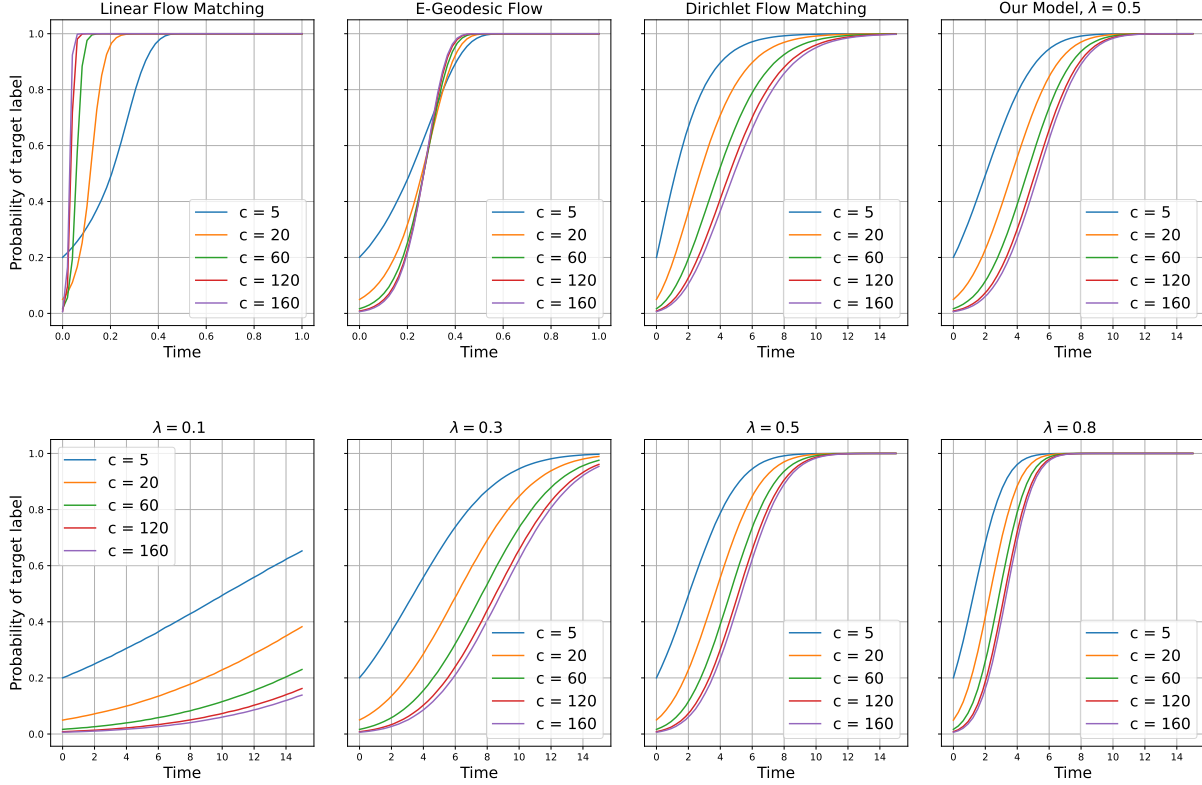


FIGURE 4.6. *Top row:* Plots of conditional densities paths  $t \mapsto p_t(\cdot|\beta)$  for various models. *Bottom row:* Impact of the rate parameter  $\lambda$  of our approach (replication of Figure 3.2 to ease visual comparison).

In practice,  $W \sim \nu_{t_{\max}}$  is typically close to a discrete Dirac already, so rounding has little impact on the represented joint distribution. Nevertheless, the rounding process is formally a different model than  $\tilde{p} = \mathbb{E}_{W \sim \nu_{t_{\max}}}[T(W)]$ , which we explicitly distinguish for the purpose of computing likelihoods. Recall the definition (3.31) of subsets  $r_\beta \subseteq \mathcal{W}$  with each  $W \in r_\beta$  assigning the largest probability to the labels  $\beta$ . The points in  $r_\beta$  are also the ones which round to  $\overline{W}_\beta$ <sup>3</sup>. Thus, the labeling  $\beta \in [c]^n$  has likelihood

$$\tilde{p}_\beta^r = \mathbb{E}_{W \sim \nu_{t_{\max}}}[\mathbf{1}_{r_\beta}(W)] = \mathbb{P}_{\nu_{t_{\max}}}(r_\beta) \quad (\text{B.1})$$

under the rounding model  $\tilde{p}^r$ , with  $\mathbf{1}_{r_\beta}$  denoting the indicator function of  $r_\beta$ . This is numerically similar to the likelihood under our original model

$$\tilde{p}_\beta = \mathbb{E}_{W \sim \nu_\infty}[T(W)_\beta] \quad (\text{B.2})$$

and matches it in the limit  $t \rightarrow \infty$ , provided that (almost) every trajectory  $W(t)$  approaches an extreme point of  $\overline{\mathcal{W}}$  under the learned assignment flow dynamics.

We will now devise an importance sampling scheme for efficient and numerically stable approximation of the integral in (B.1), that analogously applies to (B.2). Let  $\varrho$  be a proposal distribution with full support on

<sup>3</sup>The sets  $r_\beta$  technically overlap on the boundary, but all intersections have measure zero.

$\mathcal{W}$  which has most of its mass concentrated around a point  $q_\beta \in \mathcal{W}$  close to  $\overline{W}_\beta$ . Then

$$\mathbb{P}_{\nu_{t_{\max}}}(r_\beta) = \mathbb{E}_{W \sim \varrho} \left[ 1_{r_\beta}(W) \frac{\nu_{t_{\max}}(W)}{\varrho(W)} \right] \quad (\text{B.3})$$

where we assumed that both  $\nu_{t_{\max}}$  and  $\varrho$  have densities with respect to the Lebesgue measure and used again the symbols  $\nu_{t_{\max}}$  and  $\varrho$  to denote these densities. The rationale behind this construction is that, since we learned  $\nu_{t_{\max}}$  to concentrate close to points  $\overline{W}_\beta$ , drawing most samples close to  $q_\beta$  will reduce the estimator variance compared to sampling (B.1) directly. In high dimensions, the quantities in (B.3) are prone to numerical underflow, which motivates the transformation

$$\log \mathbb{P}_{\nu_{t_{\max}}}(r_\beta) = \log \mathbb{E}_{W \sim \varrho} \left[ 1_{r_\beta}(W) \frac{\nu_{t_{\max}}(W)}{\varrho(W)} \right] \quad (\text{B.4a})$$

$$= \log \mathbb{E}_{W \sim \varrho} \left[ \exp \left( \log 1_{r_\beta}(W) + \log \nu_{t_{\max}}(W) - \log \varrho(W) \right) \right]. \quad (\text{B.4b})$$

After replacing the expectation with a mean over samples drawn from  $\varrho$ , we can evaluate (B.4) by leveraging stable numerical implementations of the logsumexp function.

For every evaluation of the integrand, we evaluate log-likelihood under  $\varrho$  in closed form as well as log-likelihood under  $\nu_{t_{\max}}$  through numerical integration backward in time, leveraging the instantaneous change of variables (3.56) and Hutchinson's trace estimator. Note the conventions  $\log 0 = -\infty$  and  $\exp(-\infty) = 0$  employed in (B.4). The analogous expression for (B.1) reads

$$\log \tilde{p}_\beta = \log \mathbb{E}_{W \sim \varrho} \left[ \exp \left( \log T(W)_\beta + \log \nu_{t_{\max}}(W) - \log \varrho(W) \right) \right] \quad (\text{B.5})$$

and we can further expand

$$\log T(W)_\beta = \log \prod_{i \in [n]} W_{i, \beta_i} = \sum_{i \in [n]} \log W_{i, \beta_i} \quad (\text{B.6})$$

to avoid numerical underflow.

## REFERENCES

- [Agr13] A. Agresti, *Categorical Data Analysis*, 3rd ed., Wiley, 2013.
- [Ait82] J. Aitchinson, *The Statistical Analysis of Compositional Data*, J. Royal Statistical Soc. B **2** (1982), 139–177.
- [AN00] S.-I. Amari and H. Nagaoka, *Methods of Information Geometry*, Amer. Math. Soc. and Oxford Univ. Press, 2000.
- [ÅPSS17] F. Åström, S. Petra, B. Schmitzer, and C. Schnörr, *Image Labeling by Assignment*, Journal of Mathematical Imaging and Vision **58** (2017), no. 2, 211–238.
- [BCA<sup>+</sup>24] B. Boll, J. Cassel, P. Albers, S. Petra, and C. Schnörr, *A Geometric Embedding Approach to Multiple Games and Multiple Populations*, preprint arXiv:2401.05918 (2024).
- [BGAS24] B. Boll, D. Gonzalez-Alvarado, and C. Schnörr, *Generative Modeling of Discrete Joint Distributions by E-Geodesic Flow Matching on Assignment Manifolds*, preprint arXiv:2402.07846 (2024).
- [BGM09] G. Beylkin, J. Garcke, and M. J. Mohlenkamp, *Multivariate Regression and Machine Learning with Sums of Separable Functions*, SIAM J. Sci. Comput. **31** (2009), no. 3, 1840–1857.
- [BSGA<sup>+</sup>23] B. Boll, J. Schwarz, D. Gonzalez-Alvarado, D. Sitenko, S. Petra, and C. Schnörr, *Modeling Large-scale Joint Distributions and Inference by Randomized Assignment*, Scale Space and Variational Methods in Computer Vision (SSVM) (L. Calatroni, M. Donatelli, S. Morigi, M. Prato, and M. Santacesaria, eds.), LNCS, no. 14009, Springer, 2023, pp. 730–742.
- [BSS21] B. Boll, J. Schwarz, and C. Schnörr, *On the Correspondence between Replicator Dynamics and Assignment Flows*, SSVM 2021: Scale Space and Variational Methods in Computer Vision, LNCS, vol. 12679, Springer, 2021, pp. 373–384.
- [CAN22] R. T. Q. Chen, B. Amos, and M. Nickel, *Semi-Discrete Normalizing Flows through Differentiable Tessellation*, NeurIPS, 2022.
- [CDLS99] R. G. Cowell, A. P. Dawid, S. L. Lauritzen, and D. J. Spiegelhalter, *Probabilistic Networks and Expert Systems*, Springer, 1999.
- [CL23] R. T. Q. Chen and Y. Lipman, *Riemannian Flow Matching on General Geometries*, preprint arXiv:2302.03660 (2023).
- [COR<sup>+</sup>16] M. Cordts, M. Omran, S. Ramos, T. Rehfeld, M. Enzweiler, R. Benenson, U. Franke, S. Roth, and B. Schiele, *The Cityscapes Dataset for Semantic Urban Scene Understanding*, Proc. of the IEEE Conference on Computer Vision and Pattern Recognition (CVPR), 2016.
- [CRBD18] R. T. Q. Chen, Y. Rubanova, J. Bettencourt, and D. Duvenaud, *Neural Ordinary Differential Equations*, Proc. NeurIPS, 2018.
- [CT06] T. M. Cover and J. A. Thomas, *Elements of Information Theory*, 2nd ed., John Wiley & Sons, 2006.
- [DKP<sup>+</sup>24] O. Davis, S. Kessler, M. Petrache, I. I. Ceylan, M. Bronstein, and A. J. Bose, *Fisher Flow Matching for Generative Modeling over Discrete Data*, preprint arXiv:2405.14554 (2024).
- [DN21] Prafulla Dhariwal and Alexander Quinn Nichol, *Diffusion models beat GANs on image synthesis*, Advances in Neural Information Processing Systems (A. Beygelzimer, Y. Dauphin, P. Liang, and J. Wortman Vaughan, eds.), 2021.
- [DP80] J. R. Dormand and P. J. Prince, *A Family of Embedded Runge-Kutta Formulae*, J. Comput. Appl. Math. **6** (1980), no. 1, 19–26.
- [DSDB17] L. Dinh, J. Sohl-Dickstein, and S. Bengio, *Density Estimation Using Real NVP*, ICLR, 2017.
- [DSS09] M. Drton, B. Sturmfels, and S. Sullivant, *Lecture on Algebraic Statistics*, Oberwolfach Seminars, vol. 39, Birkhäuser, 2009.
- [Fer73] T. S. Ferguson, *A Bayesian Analysis of Some Nonparametric Problems*, Ann. Statistics **2** (1973), no. 1, 209–230.
- [GCB<sup>+</sup>19] W. Grathwohl, R. T. Q. Chen, J. Bettencourt, I. Sutskever, and D. Duvenaud, *FFJORD: Free-Form Continuous Dynamics for Scalable Reversible Generative Models*, ICLR, 2019.
- [GKT13] L. Grasedyck, D. Kressner, and C. Tobler, *A Literature Survey of Low-Rank Tensor Approximation Techniques*, GAMM Mitt. **36** (2013), no. 1, 53–78.
- [GMS06] D. Geiger, C. Meek, and B. Sturmfels, *On the Toric Algebra of Graphical Models*, The Annals of Statistics **34** (2006), no. 3, 1463–1492.
- [Hac14] W. Hackbusch, *Numerical Tensor Calculus*, Acta Numerica **23** (2014), 651–742.
- [Har92] J. Harris, *Algebraic Geometry: A First Course*, Springer, 1992.
- [HCS<sup>+</sup>19] J. Ho, X. Chen, A. Srinivas, Y. Duan, and P. Abbeel, *Flow++: Improving flow-based generative models with variational dequantization and architecture design*, Proc. ICML, vol. PMLR 97, 2019, pp. 2722–2730.
- [HLW06] E. Hairer, C. Lubich, and G. Wanner, *Geometric Numerical Integration*, Springer, 2006.
- [HNJ<sup>+</sup>21] E. Hoogeboom, D. Nielsen, P. Jaini, P. Forré, and M. Welling, *Argmax Flows and Multinomial Diffusion: Learning Categorical Distributions*, NeurIPS, 2021.
- [HNW08] E. Hairer, S.P. Nørsett, and G. Wanner, *Solving Ordinary Differential Equations I*, 3rd ed., Springer, 2008.
- [HS98] J. Hofbauer and K. Sigmund, *Evolutionary Games and Population Dynamics*, Cambridge University Press, 1998.

- [Hut89] M. F. Hutchinson, *A Stochastic Estimator of the Trace of the Influence Matrix for Laplacian Smoothing Splines*, Communications in Statistics-Simulation and Computation **18** (1989), no. 3, 1059–1076.
- [JK77] N. L. Johnson and S. Kotz, *Urn Models and Their Application*, John Wiley & Sons, 1977.
- [KB09] T. G. Kolda and B. W. Bader, *Tensor Decompositions and Applications*, SIAM Review **51** (2009), no. 3, 455–500.
- [KF09] D. Koller and N. Friedman, *Probabilistic Graphical Models: Principles and Techniques*, MIT Press, 2009.
- [KPB21] I. Kobyzev, S.J. D. Prince, and M. A. Brubaker, *Normalizing Flows: An Introduction and Review of Current Methods*, IEEE Trans. Pattern Anal. Mach. Intell. **43** (2021), no. 11, 3964–3979.
- [Lan12] J. M. Landsberg, *Tensors: Geometry and Applications*, Amer. Math. Soc., 2012.
- [Lau96] S. L. Lauritzen, *Graphical Models*, Clarendon Press, Oxford, 1996.
- [LCB10] Yann LeCun, Corinna Cortes, and CJ Burges, *Mnist handwritten digit database*, ATT Labs [Online]. Available: <http://yann.lecun.com/exdb/mnist> **2** (2010).
- [LCBH<sup>+</sup>23] Y. Lipman, R. T. Q. Chen, H. Ben-Hamu, M. Nickel, and M. Le, *Flow Matching for Generative Modeling*, ICLR, 2023.
- [LM18] W. Li and G. Montufar, *Natural gradient via optimal transport*, Information Geometry **2** (2018), no. 1, 181–214.
- [LSX09] S. Lin, B. Sturmfels, and Z. Xu, *Marginal Likelihood Integrals for Mixtures of Independence Models*, J. Machine Learning Research **10** (2009), 1611–1631.
- [MK99] H. Munthe-Kaas, *High Order Runge-Kutta Methods on Manifolds*, Applied Numerical Mathematics **29** (1999), no. 1, 115–127.
- [PNR<sup>+</sup>21] G. Papamakarios, E. Nalisnick, D.J. Rezende, S. Mohamed, and B. Lakshminarayanan, *Normalizing Flows for Probabilistic Modeling and Inference*, J. Machine Learning Research **22** (2021), no. 57, 1–64.
- [RH21] L. Ruthotto and E. Haber, *An Introduction to Deep Generative Modeling*, GAMM Mitt. **44** (2021), no. 2, 24 pages.
- [San15] F. Santambrogio, *Optimal Transport for Applied Mathematicians*, Birkhäuser, 2015.
- [Sch20] C. Schnörr, *Assignment Flows*, Variational Methods for Nonlinear Geometric Data and Applications (P. Grohs, M. Holler, and A. Weinmann, eds.), Springer, 2020, pp. 235–260.
- [SJW<sup>+</sup>24] H. Stark, B. Jing, C. Wang, G. Corso, B. Berger, R. Barzilay, and T. Jaakkola, *Dirichlet Flow Matching with Applications to DNA Sequence Design*, preprint arXiv:2402.05841 (2024).
- [SKCK17] T. Salimans, A. Karpathy, X. Chen, and D. P. Kingma, *PixelCNN++: Improving the pixelCNN with discretized logistic mixture likelihood and other modifications*, ICLR, 2017.
- [Stu05] M. Studený, *On Probabilistic Conditional Independence Structures*, Springer, 2005.
- [Sul18] S. Sullivant, *Algebraic Statistics*, American Mathematical Society, 2018.
- [TvdOB16] L. Theis, A. van den Oord, and M. Bethge, *A Note on the Evaluation of Generative Models*, ICLR, 2016.
- [UML13] B. Uria, I. Murray, and H. Larochelle, *RNAE: The Real-Valued Neural Autoregressive Density-Estimator*, NIPS, 2013.
- [Vil09] C. Villani, *Optimal Transport: Old and New*, Springer, 2009.
- [ZSPS20] A. Zeilmann, F. Savarino, S. Petra, and C. Schnörr, *Geometric Numerical Integration of the Assignment Flow*, Inverse Problems **36** (2020), no. 3, 034004 (33pp).
- [Zwi16] P. Zwiernik, *Semialgebraic Statistics and Latent Tree Models*, CRC Press, 2016.
- [ZZS22] A. Zern, A. Zeilmann, and C. Schnörr, *Assignment Flows for Data Labeling on Graphs: Convergence and Stability*, Information Geometry **5** (2022), 355–404.

(B. Boll, D. Gonzalez-Alvarado) INSTITUTE FOR MATHEMATICS, IMAGE AND PATTERN ANALYSIS GROUP, HEIDELBERG UNIVERSITY, GERMANY

Email address: [daniel.gonzalez@iwr.uni-heidelberg.de](mailto:daniel.gonzalez@iwr.uni-heidelberg.de)

URL: <https://ipa.math.uni-heidelberg.de>

(S. Petra) MATHEMATICAL IMAGING GROUP, DEPARTMENT OF MATHEMATICS & CENTRE FOR ADVANCED ANALYTICS AND PREDICTIVE SCIENCES (CAAPS), UNIVERSITY OF AUGSBURG, UNIVERSITÄTSSTR. 14, 86159 AUGSBURG, GERMANY

Email address: [Stefania.Petra@uni-a.de](mailto:Stefania.Petra@uni-a.de)

URL: <https://www.uni-augsburg.de/de/fakultaet/mntf/math/prof/mig/>

(C. Schnörr) INSTITUTE FOR MATHEMATICS & RESEARCH STATION GEOMETRY AND DYNAMICS, IMAGE AND PATTERN ANALYSIS GROUP, HEIDELBERG UNIVERSITY, GERMANY

Email address: [schnoerr@math.uni-heidelberg.de](mailto:schnoerr@math.uni-heidelberg.de)

URL: <https://ipa.math.uni-heidelberg.de>